CANMET

Canada Centre for Mineral and Energy Technology
Centre canadien de la technologie des minéraux et de l'énergie

REPORT 81-4E

THE EFFECTS OF PORE SIZE IN MoO_3-CoO-Al_2O_3 HYDROCRACKING CATALYSTS

A.H. HARDIN, M. TERNAN and R.H. PACKWOOD

ENERGY RESEARCH PROGRAM
ENERGY RESEARCH LABORATORIES

AUGUST 1981

Energy, Mines and Resources Canada
Énergie, Mines et Ressources Canada

Canada

Available in Canada through

Authorized Bookstore Agents
and other bookstores

or by mail from

Canadian Government Publishing Centre
Supply and Services Canada
Hull, Quebec, Canada K1A 0S9

CANMET
Energy, Mines and Resources Canada,
555 Booth St.,
Ottawa, Canada K1A 0G1

or through your bookseller

Catalogue No. M38-13/81-4E
ISBN 0-660-11065-2

Canada: $3.75
Other countries: $4.50

Price subject to change without notice.

En vente au Canada par l'entremise de nos

agents libraires agréés
et autres librairies

ou par la poste au:

Centre d'édition du gouvernement du Canada
Approvisionnements et Services Canada
Hull, Québec, Canada K1A 0S9

CANMET
Énergie, Mines et Resources Canada,
555, rue Booth
Ottawa, Canada K1A 0G1

ou chez votre libraire.

Nº de catalogue M38-13/81-4E
ISBN 0-660-11065-2

Canada: $3.75
Hors Canada: $4.50

Prix sujet à changement sans avis préalable.

THE EFFECTS OF PORE SIZE IN MoO_3-CoO-Al_2O_3 HYDROCRACKING CATALYSTS

by

A.H. Hardin*, M.Ternan** and R.H. Packwood***

ABSTRACT

Effects of variations in mean pore diameter in four series of catalysts have been determined for hydrodesulphurization, hydrodenitrogenation and conversion reactions of Athabasca bitumen. Standard tests were made on a blank alumina support and three cobalt/molybdenum/alumina catalyst series having the compositions 1.1:2.2, 4.4:8.8 and 3.0:15.0 *m* % CoO:MoO_3, respectively. Catalysts were prepared by solution impregnation of AlOOH, followed by extrusion, dehydration and calcining at a series of temperatures between 500°C and 1100°C. Several median pore diameter ranges were tested for each catalyst.

Some physical properties of the prepared catalysts were measured. Median pore diameter distributions, determined by Hg penetration, had values between 7.0 and 100.0 nm. Pore volumes varied between 0.25 and 0.65 mLg^{-1}. Surface areas, determined by nitrogen BET (Brunauer, Emmett and Teller) were found to vary from 1 to 200 m^2g^{-1}. Used catalysts were de-oiled by benzene extraction prior to analysis by electron microprobe and prior to analysis for deposited coke content.

A 25.4-mm diameter, 0.381 m long stainless-steel tubular reactor was filled with a fixed bed of catalyst. Premixed bitumen and hydrogen were bottom-fed to the reactor at a liquid hourly space velocity of 1.0. Standard operating conditions of 13.9 MPa, 440°C and 800 L of H_2 per litre of feed were used in all cases. The catalysts were all presulphided with bitumen immediately prior to the studied reactions.

Mounted and sectioned catalyst specimens were analyzed radially for distributions of Fe, Ni, V and S. The electron microprobe analyses indicated distinct variations in the radial distributions of Fe, Ni, V and S across the catalysts.

Effects of pore size variations on hydrodesulphurization, hydrodenitrogenation, pitch conversion and coke formation were determined. The results indicated maxima for mass per cent sulphur removal for pores near 15 nm for two catalysts. As well, the rates per unit area for S and N removal increased as mean pore diameters increased to about 50 nm, after which the rates appeared to be constant.

---

*Former research scientist, (presently senior research chemist at Syncrude Canada Limited, Research Department, Edmonton), **Head, Catalysis Section, Synthetic Fuels Research Laboratory, Energy Research Laboratories, Canada Centre for Mineral and Energy Technology (CANMET), and ***Research scientist, Physical Metallurgy Research Laboratories, CANMET, Energy, Mines and Resources Canada, Ottawa.

LES EFFETS DE LA TAILLE DES PORES SUR LES CATALYSEURS MoO_3-CoO-Al_2O_3 UTILISÉS DANS LE PROCÉDÉ D'HYDROCRAQUAGE

par

A.H. Hardin*, M. Ternan** et R.H. Packwood***

RESUMÉ

Les effets de variations du diamètre moyen des pores de quatre séries de catalyseurs ont été déterminés pour les réactions d'hydrodésulfuration, d'hydrodénitrogénation et de conversion du bitume d'Athabasca. Les essais normalisés ont été effectués sur un soutien d'alumine à blanc et trois séries de catalyseurs de cobalt/molybdène/alumine ayant des compositions respectives de $CoO:MoO_3$ de 1,1:2,2, 4,4:8,8 et 3,0:15,0 p. cent *m*. Les catalyseurs ont été préparés en imprégnant le AlOOH de solution , suivi de l'extrusion, la déshydratation et la calcination à une gamme de températures entre 500°C et 1100°C. Plusieurs gammes de diamètre médian des pores ont été soumises à des essais pour chacun des catalyseurs.

Certaines propriétés physiques des catalyseurs ainsi préparés ont été mesurées. La valeur de la distribution du diamètre moyen des pores, telle que déterminée par la pénétration du Hg, pouvait varier entre 7,0 et 100,0 nm. Le volume des pores pouvait varier entre 0,25 et 0,65 mLg^{-1}. Les aires de surface, déterminées par la méthode BET (Brunauer, Emmett et Teller) à l'azote, pouvaient varier de 1 à 200 m^2g^{-1}. Les catalyseurs usés étaient soumis à une extraction de l'huile par le benzène avant d'être analysés à la microsonde électronique et avant d'être analysés pour son contenu de coke.

Un réacteur tubulaire en acier inoxydable de 0,381 m de long et ayant un diamètre de 25,4 mm a été rempli de catalyseurs en lit fixe. Le réacteur était alimenté par le fond de bitume et d'hydrogène préalablement mélangé, à une vitesse spatiale liquide horaire de 1,0. Des critères de fonctionnement étaient établis d'avance à 13,9 MPa, 440°C et 800 L de H_2 par litre d'alimentation dans tous les cas. Les catalyseurs avaient tous été pré-sulfurés à l'aide de bitume l'instant avant les réactions étudiées.

Les échantillons de catalyseurs fixés et profilés ont été analysés radialement en fonction des distributions de Fe, Ni, V et S. Les analyses à la microsonde électronique ont indiqué des variations distinctes dans les distributions radiales de Fe, Ni, V et S sur les catalyseurs.

Les effets des variations de la taille des pores sur l'hydrodésulfuration, l'hydrodénitrogénation, la conversion du brai et la formation du coke ont été déterminés. Les résultats ont indiqué un maxima pour l'enlèvement du soufre en pourcentage mol. pour les pores près de 15 nm dans le cas de deux catalyseurs. De plus, le taux d'enlèvement du S et du N par unité d'aire augmente avec l'augmentation des diamètres moyens des pores jusqu'à 50 nm, après quoi le taux semble constant.

---

*Ancien chercheur scientifique, (présentement chimiste de recherche principal à Syncrude Canada Limited, Département de recherche, Edmonton), **Chef, Section de la catalyse, Laboratoire de recherche sur les carburants synthétiques, Laboratoires de recherche énergétique, Centre canadien de la technologie des minéraux et de l'énergie (CANMET), et ***Chercheur scientifique, Laboratoires de recherche en métallurgie physique, CANMET, Énergie, Mines et Ressources Canada, Ottawa.

CONTENTS

	Page
ABSTRACT	i
RESUMÉ	ii
INTRODUCTION	1
EXPERIMENTAL PROCEDURE	2
RESULTS AND DISCUSSION	4
Initial Catalyst Properties	5
Converted Bitumen Properties	12
(a) Relative densities	12
(b) H:C ratio	13
(c) Conversion of pitch and asphaltenes	14
(d) Aromatics, olefins and paraffins	16
(e) Sulphur and nitrogen conversion	17
(f) Vanadium, nickel and iron conversions	20
(g) Catalyst deposited metals	22
(h) Catalyst coke composition	23
The Influence of Diffusion on Reaction Rate	25
(a) Combined effects of pore size and surface area on diffusion	25
(b) Basis of calculation	25
(c) Sulphur removal	26
(d) Nitrogen removal	26
(e) Diffusion coefficients and effectiveness factors	27
CONCLUSIONS	28
ACKNOWLEDGEMENTS	29
REFERENCES	29
APPENDIX A - CATALYST MEASUREMENTS AND PROPERTIES OF THE LIQUID PRODUCT	A-33

TABLES

1. Properties of Athabasca bitumen feedstock	3
2. Solid phases of the fresh catalysts	5
3. Colour and composition of fresh catalysts	7
4. Colour and composition of fresh catalysts	8
5. Colours of pure components as a function of temperature	9
6. Heteroatom concentrations in asphaltenes and total feedstock	15
A-1 Catalyst measurements	A-35
A-2 Properties of the liquid product	A-36

FIGURES

		Page
1.	Relationship between calcining temperature, °C, and the median pore diameter of the fresh catalyst, nm	6
2.	Catalyst pore volume, mL/g, from mercury penetration measurements versus median pore diameter, nm	10
3.	Catalyst surface area, m^2/g, versus median pore diameter, nm	10
4.	Total catalyst surface area in the reactor, m^2, versus median pore diameter, nm	10
5.	Catalyst pore volume, mL/g, versus median pore diameter, nm	10
6.	Density of catalyst extrudates, g/mL, versus median pore diameter, nm	11
7.	Density of catalyst extrudates, g/mL, versus median pore diameter, nm	11
8.	Mass per cent CoO on catalyst versus median pore diameter, nm	12
9.	Mass per cent MoO_3 on catalyst versus median pore diameter, nm	12
10.	Total mass of catalyst in the reactor versus median pore diameter, nm	13
11.	Total mass of catalyst in the reactor versus median pore diameter, nm	13
12.	Relative density versus median pore diameter, nm	14
13.	Relative density versus median pore diameter, nm	14
14.	Hydrogen to carbon atomic ratio in the liquid product versus median pore diameter, nm	15
15.	Mass per cent asphaltenes removed from the liquid versus median pore diameter, nm	15
16.	Mass per cent +525°C pitch converted versus median pore diameter, nm	16
17.	Mass per cent +525°C pitch converted versus median pore diameter, nm	16
18.	Per cent of aromatic carbon atoms in the liquid versus median pore diameter, nm	17
19.	Per cent of aromatic carbon atoms in the liquid versus median pore diameter, nm	17
20.	Per cent of paraffinic carbon atoms in the liquid product versus median pore diameter, nm	18
21.	Per cent of paraffinic carbon atoms in the liquid product versus median pore diameter, nm	18
22.	Mass per cent sulphur removed from the liquid product versus median pore diameter, nm	19
23.	Mass per cent sulphur removed from the liquid product versus median pore diameter, nm	19
24.	Mass per cent nitrogen removed from the liquid product versus median pore diameter, nm	19
25.	Mass per cent nitrogen removed from the liquid product versus median pore diameter, nm	19
26.	Mass per cent vanadium removed from the liquid product versus median pore diameter, nm	20

FIGURES (cont'd)

Page

27. Mass per cent vanadium removed from the liquid product versus median pore diameter, nm 20

28. Mass per cent nickel removed from the liquid product versus median pore diameter, nm 20

29. Mass per cent nickel removed from the liquid product versus median pore diameter, nm 20

30. Mass per cent iron removed from the liquid product versus median pore diameter, nm 21

31. Mass per cent iron removed from the liquid product versus median pore diameter, nm 21

32. Relative intensity or metals concentration (A = vanadium, B = nickel, C = iron) versus radial position in the catalyst extrudate, r/R 22

33. Radial position r/R in the catalyst having maximum vanadium deposition, maximum relative peak height, rph, versus median pore diameter, nm 23

34. Atomic hydrogen to carbon ratio in used catalyst versus median pore diameter, nm 23

35. Amount of carbon on the used catalyst, mg/m^2, versus median pore diameter, nm 24

36. Amount of nitrogen on the used catalyst, mg/m^2, versus median pore diameter, nm 24

37. Total surface area in reactor, m^2, versus median pore diameter, nm 26

38. Atoms sulphur removed per ks per nm^2 versus median pore diameter, nm 27

39. Atoms nitrogen removed per ks per nm^2 versus median pore diameter, nm ... 27

INTRODUCTION

Utilization of bitumens and heavy oils is severely limited in conventional refinery technology by the nature of these feedstocks. A typical bitumen separated from Athabasca oil sands has a 55% +525°C fraction, 15 *m* % asphaltenes, 300 µg/g V, 90 µg/g Ni, 4.5 *m* % S, 0.41 *m* % N, and and an H:C ratio of 1.51. These properties are like those of vacuum tower residuum, normally considered a low value byproduct.

Current upgrading strategies, employed by SUNCOR (1) and Syncrude (2), involve coking, i.e., carbon withdrawal, to improve the H:C ratio and the average molecular mass. However, coking processes for a 16 400 m^3/d plant produce large volumes of waste coke, upwards of 910 t/d (1,2). This represents over 4910 m^3/d of lost potential liquid production and a considerable loss of annual revenue. The advantage of the coking processes is that they have been demonstrated on a commercial scale.

The alternative strategy of hydrogen addition (hydrocracking and hydrotreating or hydrogenation and hydrogenolysis) has been pursued actively by several organizations, i.e., Hydrocarbon Research Incorporated with H-Oil, Lummus-Cities Services with L-C Fining, Universal Oil Products and others. The first two utilize commercially available hydrodesulphurization catalysts. However, catalyst deactivation, consumption, and replacement costs can become significant factors in determining the economic viabilities of these processes. Only two commercial plants are in operation - H-Oil in Kuwait (3) and L-C Fining in Mexico (4).

From the point of view of hydrodesulphurization (HDS), hydrodemetallization (HDM), and hydrodenitrogenation (HDN) of bitumens and heavy oils, the use of $CoMoAl_2O_3$ catalysts has implications that are impressive. Using published data on the average HDS catalyst production and the amounts of sulphur produced by them, it can be estimated that a single 16 400 m^3/d plant processing bitumen would have an annual consumption of 3-4.5 Gg of catalyst. The Canadian requirement of catalyst for 10 such plants by the year 2000 would have a large impact on the world Co and Mo supply.

Thus alternative refining strategies must be developed or significant improvements must be achieved in $CoMoAl_2O_3$ catalyst lifetime, effectiveness, and regenerability.

Several groups have made significant progress along these lines (5-10). Energy, Mines and Resources Canada is looking at several aspects of the problems in a continuing program of catalyst research and development.

The present work on mass transfer limitations in the catalyst pore systems is one aspect of that program.

Catalytic hydrogenation and hydrogenolysis of Athabasca bitumen using conventional commercial catalysts is difficult. The high concentrations of iron, vanadium and nickel, the high +525°C fraction, and high asphaltene components lead to rapid catalyst deactivation. The main mechanisms are believed to be the formation of "coke" on external and internal catalyst surfaces and the precipitation of poisoning metals onto the catalytically active surfaces. Coke formation in the macropores and mesopores decreases pore size and inhibits mass transfer beyond the point where the maximum chemical reaction rate can occur, i.e., by decreasing the flow of reactant molecules to the reaction site and thus decreasing the net concentration in the rate equation $\frac{dc}{dt}$ term. The chemical reaction rate is thus less than optimum.

Vanadium metal deposition in the pore system, especially at pore mouths, has a similar effect. More important, however, is its effect in masking the catalytic sites and in modifying the chemistry of the sites responsible for the catalytic action. These resulting chemical species, probably involving V, Co, Mo, and O(S), are believed to be less active chemically than the original Co, Mo, O(S) species; that is, the reaction sites are poisoned (11).

Previous work in the authors' laboratory has indicated that metals deposition occurs mainly at or near the external catalyst skin (12). Some increase in catalyst life and effectiveness might be expected if the metals deposition and coke

formation could be minimized and spread as uniformly as possible over the whole of the catalyst active surface area. The narrowness of mesopores ~7.5 nm in conventional catalysts inhibits the diffusion of reactants. This is especially important for asphaltene micelles with diameters of 1 - 2 nm and very large molecules such as metal complexing porphyrins and polycyclic aromatics (13).

Evidence that the coking inhibitions occur mainly in the mesopores, and possibly in micropores, comes from the fact that the major losses in pore volumes for used compared with unused catalysts, occur in the mesopore range (14). At the same time the macropore volumes are little affected. Mass transfer limitations in the pore system are thought to be major hindrances to higher catalyst effectiveness in view of the large asphaltene component of bitumens. High average molecular masses of 6000 and relatively high concentrations of geometrically large polycyclic aromatic structures in bitumens suggest that diffusion in the system of intergranular cracks and intragranular pores limits the net chemical activity, i.e., the catalyst effectiveness. Studies by other workers using coal slurries (15,16) and petroleum residua (17,18) have indicated that there is merit in using catalysts with mesopore sizes that promote enhanced mass transfer. Prior evaluations of the bottom feed, concurrent flow reaction system have shown that the effects of mass transfer limitations external to the catalyst are minimal.

Several methods have been suggested for improving the short catalyst life and high operating cost expected for hydrogenation and hydrogenolysis of bitumen. In this report results are given from the investigation of the effects of variation in catalyst macropore and mesopore sizes on several measures of bitumen conversion.

A series of catalysts was prepared with N_2 BET (nitrogen Brunauer, Emmett and Teller) surface areas in the range 180 m^2g^{-1} to 2 m^2g^{-1}, total pore volumes in the range 0.60 to 0.46 mLg^{-1}, and median macropore-mesopore diameters (d_p) from 7.5 nm to 3000 nm (Appendix A, Table A-1). At the same time the ratio of macropore and mesopore volumes varied. Each catalyst was reacted with bitumen under a given set of conditions to determine pore size effects on sulphur removal and reaction rate, nitrogen removal and reaction rate, metal removal, catalyst coke levels, and catalyst metal profile (radial). As well, the effects on the aromatic carbon content, hydrogento-carbon ratio, and pentane-insoluble components of the liquid products were determined. The results discussed in this paper are for four series of catalysts with nominal $CoO:MoO_3$ loadings on Al_2O_3 of: 0.0:0.0; 1.1:2.2; 4.4: 8.8; and 3.0: 15.0 *m %*.

The pore size variations were obtained by simply calcining the $Co(NO_3)_2$ - $(NH_4)_6 Mo_7O_{24} \cdot 4H_2O$:AlOOH gels. It has been assumed that the variations in solid phase of the Al_2O_3 ($\gamma \rightarrow \eta \rightarrow \Delta \rightarrow \alpha$), in the chemical species present at the surfaces, i.e., the specific Co-Mo-Al-O species formed, and in chemical, catalytic activities do not introduce large perturbations to the pore size results. As well, the changes in mechanical and physical properties that occur and will affect catalyst durability are neglected.

In spite of these shortcomings, there is reason to believe that the method of preparation is acceptable (9). The alternative of wet impregnation into precalcined Al_2O_3 presents a host of additional problems. For example, the problem of large variations in the surface concentrations of catalytically active elements would be acute. A comprehensive body of literature is developing on the roles of catalyst preparation and surface physical properties in determining catalytic activity (19-25). The role of liquid mass transfer has been less well defined.

EXPERIMENTAL PROCEDURE

The chemical and physical properties typical of the bitumen used in these experiments are given in Table 1.

The chemical preparation of the X *m %* MoO_3, Y *m %* CoO catalyst gels involved solution impregnation of high purity SB alumina (boehmite, AlOOH) with acidified solutions of ammonium paramolybdate and cobalt nitrate. The resultant

Table 1 - Properties of Athabasca bitumen feedstock

Relative density (15°C)		1.009	+525°C	*m* %	54.4
Sulphur	*m* %	4.48	Molar H:C ratio		1.51
Nitrogen	*m* %	0.41	Hydrogen	*m* %	10.68
Vanadium	*mg/g*	306	Carbon	*m* %	83.89
Nickel	*mg/g*	91	Aromatic C(a)	Atom %	25.45
Iron	*mg/g*	390	Olefinic C(a)	Atom %	0.1
Pentane insoluble	*m* %	15.0	Saturated C(a)	Atom %	74.55
Benzene insoluble	*m* %	0.52			

(a) Determined by quantitative ^{13}C and ^{1}H nmr (35).

pastes were mulled until uniform, smooth and physically stable so that suitable extrudates could be made. The 3.17-mm diameter extrudates were formed using a 5.72-mm Bonnot bench-scale extruder. After partial dehydration in air at 383 K for 6.0 h in a preheated oven, the extrudates were sealed and stored until calcined.

Catalysts with varying pore sizes were prepared from these partially dehydrated extrudates by calcination at different constant temperatures. Samples were loaded in a thin layer in shallow, vitrosil trays which were placed directly into a pre-heated muffle furnace. After calcining for 2 h at constant temperature, the samples were cooled in air, sealed and stored. One exception to this was the catalyst with a median pore diameter of 1180 nm - it was calcined for only 0.5 h at 1323 K.

The extruded catalysts thus prepared were physically characterized. Specific surface areas were determined by a standard BET H_2 gravimetric method (26). Catalyst pore volumes and pore diameters (d_p) were measured by mercury penetration using a Micromeritics Model 910 porosimeter operating at up to 348 MPa, capable of measuring pores as small as 4 nm. After being weighed in the porosimetry cell, but before loading the cell into the high pressure chamber, the catalysts were dehydrated at 393 K for one hour. This helped considerably to reduce the pump-down time of the catalyst and porosimetry chamber.

Pore diameters were calculated in the usual way using an assumed, constant contact angle of 130 degrees, the applied hydrostatic pressure, and a constant mercury surface tension of 0.474 N/m (26). The mercury used in the porosimeter was initially a redistilled technical-grade product. As the chemical composition of these catalysts is relatively constant, differences in contact angle are thought to be small. Variations in the mercury surface tension as a function of chemical contamination during a series of determinations were not taken into account.

The bitumen conversion efficacies of each catalyst were tested using a bottom fed, fixed-bed reaction system which has been used in these laboratories for some time. A constant volume of 127 mL of catalyst was charged into a 25.4-mm id stainless steel, continuous flow reactor 0.381 m long. In this study, the $CoMo/Al_2O_3$ catalysts were presulphided by exposure to bitumen for 5 h, including the periods for reactor heat-up. This was followed directly by the 2-h conversion reaction experiment at steady reactor conditions. Presulphiding was effected at 13.9 MPa, 723 K, LHSV = 1.2, and a hydrogen flow rate of 844 L/L bitumen feed. The bitumen was pumped at 328 K by precalibrated Ruska pumps to preheaters at the reactor base. The reactor had an axial temperature profile of ±5 K over the length of the catalyst bed. The 2-h experiments described here were conducted under the same reaction conditions as for presulphiding except that the temperature was lowered to 713 K.

To distinguish the net changes in the

catalytic reaction rates, as opposed to the overall thermal plus catalytic effects, a simulated thermal base case was studied. Soft iron rod of 3.2 mm diameter was cut so that the resulting lengths had a distribution approximating that of the extrudates. As with catalyst extrudates, 127 mL of these steel "extrudates" was loaded into the reactor. A normal presulphiding experimental reaction sampling regime was followed. Analyses from this run were assumed to be indicative of a purely thermal run.

Liquid products from the reaction experiments were withdrawn for analysis from a separate sample receiver vessel (Appendix A, Table A-2). Sulphur and vanadium contents were analyzed by X-ray fluorescence using an Inax Instruments Ltd. model 311 spectrometer. Carbon, nitrogen and hydrogen contents were measured by sample combustion using a Perkin-Elmer model 240 analyzer. Nickel and iron in the liquids were determined by wet ashing and atomic absorption spectrophotometry. The unconverted asphaltenes - in this case pentane insolubles - were determined by a modification of ASTM method 2042-76. Benzene insolubles, largely mineral matter, were also determined in this way. The conversions of pitch were determined by either an 8-point or 2-point modified Hempel distillation. The results are reported as m % +525°C converted. The percentage of total carbon present as aromatics, olefins, and saturated carbon was determined by quantitative ^{13}C and ^{1}H nuclear magnetic resonance (nmr) using methods recently developed in these laboratories (27).

Used catalyst samples were analyzed for residual carbon, hydrogen, nitrogen and metals in catalyst coke after Soxhlet benzene extraction of the used catalysts. The extractions were continued until the returning solvent was visually clear. Solvent and residual liquids were removed by heating in air at 393 K for 18 h. The remaining carbon, nitrogen and hydrogen from "coke" on the dried catalyst were determined by combustion, as before.

Radial distributions for iron, nickel, vanadium, molybdenum and cobalt were determined by electron microprobe analysis using a JEOL JXA-3 instrument equipped with a CPS high voltage power supply and ORTEC electronics. The profile traces for element pairs were made at 20 kV. The electron beam traversed the samples at 0.5 mm/min whereas the chart speed was 2 cm/min. The X-ray counts and digitized current, integrated over 10-s intervals, were printed out every 14 s. A beam size of 25 μm was employed as a compromise appropriate to the detail sought and the resolution on the chart. Pure metals and iron pyrites were used as reference materials.

To prepare samples for microprobe examination, short lengths were cut from central portions of the extrudates. They were impregnated with Araldite epoxy resin at 69.5 MPa, cured, cross sectioned radially, and then polished in conventional fashion. To improve sample electrical conductivity, and to decrease surface charging effects, 40-nm layers of carbon were evaporated onto the polished surfaces. As the concentrations of iron, nickel and vanadium on the catalyst are relatively low, the statistical accuracy of the data is limited.

Interference between the observed S K_α and Mo L_α X-ray lines in sulphided, used catalysts was taken into account by comparing with results from similar but oxidized unused catalysts.

Several of the calcined catalysts were analyzed for solid phase composition by powder X-ray diffraction. Diffraction patterns were recorded using a 57.3-mm Debye Scherrer camera and Co K_α radiation. The films were evaluated by comparing with ASTM standards.

RESULTS AND DISCUSSION

Determination of the effects of liquid mass transfer limitations on net chemical reaction rates is very complex. A pragmatic approach was taken and certain simplifying assumptions were made. The most important of these were:

1. changes in alumina support solid phase do not affect the chemical reaction rate;
2. changes in chemical state of the molybdenum catalyst and cobalt promoter do not affect the chemical reaction rate.

Based on these assumptions this pore size varia-

tion study will be discussed in terms of initial physical and chemical properties of the catalyst, bitumen feed and chemical and physical properties of the product, nuclear magnetic resonance, carbon type analysis, chemical and physical properties of the used catalysts, metals distribution in the used catalysts, and, finally, net chemical reaction rates for sulphur and nitrogen removal.

INITIAL CATALYST PROPERTIES

It is well known that alumina and its hydroxides can exist in many solid modifications (28,29). X-ray diffraction (XRD) patterns of a series of eight powdered catalysts were measured. The results for the 4.4 *m* % CoO:8.8 *m* % MoO_3 Al_2O_3 catalysts are shown in Table 2. These catalysts had been calcined for 2 h at fixed temperatures of between 873 K and 1323 K. That range spans the transition temperatures from η-, and γ- alumina through Δ, Θ, κ to α-Al_2O_3 (corrundum) (28,29).

The XRD data in Table 2 show the dominant > 60% phase first followed by minor phases. Below 800°C calcining the dominant phases are η- and γ-Al_2O_3 with significant portions of unstructured amorphous alumina. The latter may be due to the extremely small crystallite sizes for the smaller portion of the sample. Alternatively, it may arise from disorder induced by trapped cobalt and molybdenum oxides, i.e., perhaps a solid solution of CoO and MoO_3 in an Al_2O_3 host.

Catalysts calcined in the range from 800°C to 850°C probably contain gradations in decreasing γ, and increasing Δ, α, Θ, and κ phases. No γ Al_2O_3 was detected (< 5 *m* %) for the 850°C samples.

From calcining at 850°C to 900°C there were increasing transitions to α-Al_2O_3 and decreasing minor Θ, κ phases. Samples calcined above 900°C showed that the Al_2O_3 was present only in the α form.

These data, in conjunction with Fig. 1, can be interpreted to show that the 4.4:8.8 Co:Mo Al_2O_3 catalysts can be classified into three catalyst-support groups:

1. those with median pore diameters, d_p from 6.5 to 30 nm having gradations of η, amorphous, and γ-Al_2O_3;
2. those with d_p from 35 nm to 550 nm having gradations of Δ, α, Θ, κ and amorphous Al_2O_3;
3. those with d_p greater than 550 nm having mainly α-Al_2O_3 with minor amounts of Θ-Al_2O_3 present.

It is very clear from the above data and Tables 2

Table 2 - Solid phases of the fresh catalyst

Catalyst MB No.	Calcined temp. (°C)	Area (m^2g^{-1})	Median pore diameter (nm d_p)	Al_2O_3 phases	Comments
362	600	185	6.5	Eta, amorph	Major followed in order by minor components.
398	700	162	7.8	Eta, amorph	Similar to MB 362
365	800	57	28.8	γ	
403	850	18	88.0	Δ, α, amorph	Other also possible.
400(1)	850	4	490	α, θ,	
400(2)	850	2	530	α, κ, θ	κ, θ about equal
363	900	1	600	α, θ	similar to MB 400(1).
364	1050	1	5500	α	Co_2O_4 possible.

(1) and (2) indicate the first and second batches of catalyst

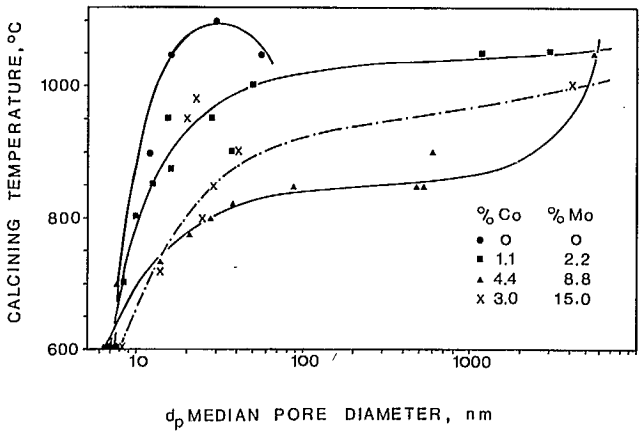

Fig. 1 - Relationship between calcining temperature, °C, and the median pore diameter of the fresh catalyst, nm.

and 4, that there are many physical changes in the alumina support as a result of pore size variation, i.e., increased calcining temperature. These solid transitions and phases vary in O-Al-O angles, Al-O distances, coordination numbers, site symmetries, and packing arrangements. The crystal systems vary from amorphous through defect spinels η, γ, monoclinic θ, orthorhombic κ, to the hexagonal layered structure of corrundum α. The biggest effect of these changes might be the variation in position of Co and Mo in the host (coordination) from defect spinel η, γ to close-packed corrundum α. The defect spinels have 21 1/3 Al atoms per unit cell randomly distributed amongst 16 octahedral and 8 tetrahedral cation sites. Thus Co^{2+}, and potentially Mo^{3+}, could be accommodated in the residual 2 2/3 sites of the support, as is discussed frequently in the literature (30). Close-packed structures do not permit this in principle.

On the other hand, most commercial catalysts are prepared by wet impregnation of the crystallized γ- or η-Al_2O_3. The catalyst used here was prepared by impregnation of wet, AlOOH, followed by dehydration. The AlOOH was transformed to Al_2O_3 with entrapped cobalt and molybdenum. We believe these trapped Co^{2+} and Mo^{3+} cations may act in manners similar to cations at defects in spinels even for the Δ, θ, κ, and, perhaps, α-Al_2O_3 forms.

High temperature calcinations affect the cobalt and molybdenum species as well as the alumina support. This was evident from the appearance of detectable amounts of Co_2O_3 in sample MB 364 (Table 2). As well, the catalysts containing Co and Mo undergo significant compositional and colour changes as a function of calcination temperature (Tables 3 and 4).

There are several possible cobalt and molybdenum oxides which could give rise to the observed colour gradations. The most important of these are listed in Table 5. The oxide MoO_3 is possible at all levels, but it is white or slightly yellow. Aside from $CoAl_2O_4$, complex mixed oxides are not included, although they are potential candidates. Possible oxidation states of cobalt are +2, +3 and +4 while molybdenums could be present in the +3, +4, +5 and +6 states. For catalysts annealed above 900°C the Co_2O_3 and Co_3O_4 oxides (Co^{+3}, $Co^{+2,+3}$) can be eliminated due to instability.

Conventional XRD powder results were unable to clearly define which of these oxides were present; more refined techniques may be able to. As well, X-ray photoelectron spectroscopy may be able to differentiate the various cobalt and molybdenum oxidation states. The latter studies are now being completed for the full range of calcination temperatures.

Calcination took place in 75 mm x 150 mm x 12 mm vitrosil trays. Normally, 4 trays of catalyst were placed in air in the 6.75-L capacity muffle furnace at one time. There was no provision for air circulation and thus evaporative losses of MoO_3 would be minimized as will be discussed later.

In one or two cases, catalysts of different chemical composition were calcined together. This may have resulted in some cross contamination.

A more severe effect appears to have been caused by miscalibrated thermocouples in the furnace. Catalysts MB 357 to MB 398 were calcined in the original furnace. The heaters were re-

Table 3 - Colour and composition of fresh catalysts

Catalyst MB No.	T_C (°C)	Area (m^2g^{-1})	d_p (nm)	V^P (mLg^{-1})	*m* % CoO	*m* % MoO_3	Colour
357	600	166	7.8	0.605	0.06	0.16	white
358	900	96	12	0.570	0.07	0.45	white
361	1050*	58	16	0.485	0.09	0.99	white
419	1100	23	29	0.360	0.00	0.03	white
359	1050	18	55	0.378	0.08	1.33	white
415	600	188	7.2	0.580	1.18	2.41	light blue
416*	600	188	7.2	0.595			
367	600	176	7.5	0.585	1.09	2.33	light blue
379*	700	157	8.5	0.600	1.09	2.53	light blue
381	800	118	10.0	0.395	1.07	2.20	light blue
382	850	99	12.5	0.500	1.05	2.17	light blue
417	950	78	15.5	0.550	1.14	2.28	light blue
418*	950	80	15.3	0.550			
384	875	79	16.0	0.465	1.06	2.19	light blue
420	1030	40	28.0	0.530	1.14	2.22	light blue
380	950	45	28.5	0.532	1.14	2.31	light blue
368	900	38	37.5	0.548	1.07	4.49	light blue-grey
383	1000	32	500	0.465	1.06	2.23	light blue
371	1050	8	1180	0.530	1.09	1.98	light grey
369	1050	2	3000	0.550	1.09	0.49	light grey

m % - mass per cent (SI)

d_p - median pore diameter

V^P - pore volume

T_C - calcining temperature

* - 0.5 h only; others for 2 h.

placed and a different thermal behaviour was observed. This is reflected in the properties for MB 399 - MB 426 in Tables 3 and 4, i.e., differences in d_p and colour for temperatures which appeared to be equivalent.

The porosity distribution of the samples varied considerably amongst macropores of > 1000 nm, large mesopores of 50-1000 nm and small mesopores of < 50 nm (Fig. 2). As well, the variation of the median pore diameters increased markedly above 500 nm (Fig. 2). Below that the approximate variation in d_p was ±10%, (Fig. 2, A and B).

The median pore diameters quoted in Tables 2-4 were taken to be equal to the value of d_p corresponding to half of the pore volume above 0.15 mLg^{-1}. The latter is the volume of macropores, i.e., those pores filled up to 1000 nm.

The strong effects of catalyst and promoter concentrations on pore size for equal calcining temperatures are seen in Fig. 1. The lowering of T^C for equal d_p follows closely the relative concentrations of cobalt, i.e., for d_p = 100 nm, T^C 0/0 > 1.1 > 3.0 > 4.4 *m* % CoO added. That is, a decrease in the calcining temperatures

Table 4 - Colour and composition of fresh catalysts

Catalyst MB No.	T_C (°C)	Area (m^2g^{-1})	d_p (nm)	V^P (mLg^{-1})	m % CoO	m % MoO_3	Colour
362	600	185	6.5	0.505	4.44	8.59	dark blue
398	700	162	7.8	0.500	4.47	8.76	dark blue
402	735	94	14	0.515	4.55	8.75	dark blue
399	775	70	21	0.502	4.39	8.77	dark blue
365	800	57	29	0.400	4.50	8.40	dark blue
401	825	28	38	0.448	4.53	8.07	blue
403	850(4)	18	88	0.395	4.56	8.35	mauve-grey
400(1)	850	4	490	0.405	4.64	7.72	grey-mauve
400(2)	850	2	530	0.430	4.55	7.58	grey-mauve
363	900	<1	600	0.430	4.58	7.58	grey
364	1050	<1	5500	0.315	4.59	4.71	med grey-black
366	1050(3)	<1	5500	0.325	4.66	7.14	med grey-black
426	600	199	5.4	0.380	3.13	15.05	blue
372	600	190	6.6	0.328	2.85	14.82	blue
376	660	90	14	0.355	2.94	14.60	blue
427	700	61	19	0.405	2.98	15.20	blue
422	775	54	20	0.415	3.10	15.12	blue-grey
423	790	44	23	0.402	3.11	15.12	grey blue
374	700	47	25	0.300	3.02	14.78	blue grey
405	725	40	29	0.305	2.97	14.85	blue grey
375	750	24	38	0.262	3.00	14.30	grey-blue
404(3)	800	3	400	0.225	-	-	
373	900	<1	3700	0.235	2.81	6.22	med grey-blue

(1) and (2) indicate the first and second batches of catalyst;
(3) 0.5 h; (4) 1 h; others 2 h.

was required to produce a given pore diameter with increasing CoO content in the catalyst.

Different dehydrated mixtures of cobalt nitrate, ammonium paramolybdate and boehmite calcined at the same T^C produced different values of d_p. Variable pH during mulling and variable retained moisture appear to affect the development of d_p, even though all samples were dehydrated for 6 h at 100°C.

From the distribution of points in Fig. 1 it can be seen that d_p's of between 100 and 500 nm were difficult to make. These would normally appear to form in the temperature ranges in which α-Al_2O_3 is forming for each concentration of CoO and MoO_3.

Specific surface area changes induced by calcining are shown in Fig. 3 and 4. In contrast to pore size variations, the effects of metal oxide concentrations on surface area is apparently minimal. The "bare" Al_2O_3 support as well as the catalyst loaded aluminas followed the same pattern. That is especially true for the smallest and largest d_p's. Caution must be used in comparing surface area changes and pore size changes. Nitrogen BET areas are often primarily associated with small pores, e.g., of less than 4 nm. How-

Table 5 - Colours of pure components as a function of temperature

Nominal *m* % CoO	Nominal *m* % MoO_3(a)	Catalyst colours/Possible species (b)				
°C		600	700	800	900	1000
0.0	0.0	white Al_2O_3				
1.1	2.2		light blue i) $CoAl_2O_4$ ii) Mo_2O_5		light blue-grey i) $CoAl_2O_4$ iv) Co_3O_4(c) ii) CoO v) Mo_2O_3 iii) Co_2O_3(c) vi) MoO_2	
4.4	8.8		dark blue i) $CoAl_2O_4$ ii) Mo_2O_5	violet grey to grey-violet i) CoO ii) Co_3O_4 iii) Co_2O_3 iv) Mo_2O_3 v) MoO_2 vi) Mo_2O_5	grey-black i) CoO iv) Mo_2O_3 ii) Co_3O_4 v) MoO_2 iii) Co_2O_3	
3.0	15.0	blue i) $CoAl_2O_4$ ii) Mo_2O_4	blue-grey to grey-blue i) $CoAl_2O_4$ iv) Mo_2O_3 ii) Co_2O_4 v) MoO_2 iii) Co_2O_3 vi) Mo_2O_5		medium grey-blue i) CoO iv) Mo_2O_3 ii) Co_3O_4(c) v) MoO_2 iii) Co_3O_4(c)	

(a) assumed chemical species for gravimetric determinations

(b) viewed at room temperature, hydrated

(c) pure compounded which decomposed above 900°C marked

ever mercury penetration porosimetry results produce data on pores greater than 4 nm.

It is recognized that the low areas have very large errors due to the method used. The McBain balance was calibrated for high area solids and is insensitive to low area material. Thus, areas of less than 3-4 m^2g^{-1} have errors of 50-100%, or more.

The pore sizes occurring in the region of greatest surface area decrease are from 12 to 19 nm. They span the range from 750 to 1000°C. Those are the temperatures at which many of the lower phases of Al_2O_3 - γ, Δ, Θ, κ - transform to α-Al_2O_3.

Total pore volume decreased by 40% for the "bare" catalyst support (Fig. 5). However, the loaded catalyst pore volume decreased less rapidly as a function of d_p. The 1.1:2.2 CoO: MoO_3 Al_2O_3 catalyst decreased by only about 10% (Fig. 4).

On a reactor-full basis the charge mass of catalyst will increase as the pore size in-

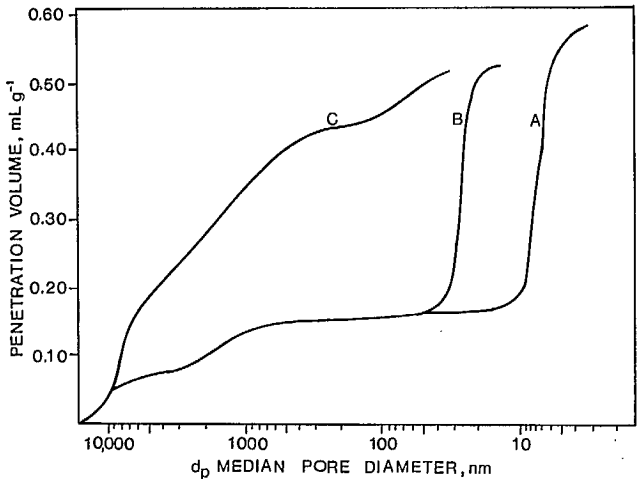

Fig. 2 - Catalyst pore volume, mL/g, from mercury penetration measurements versus median pore diameter, nm

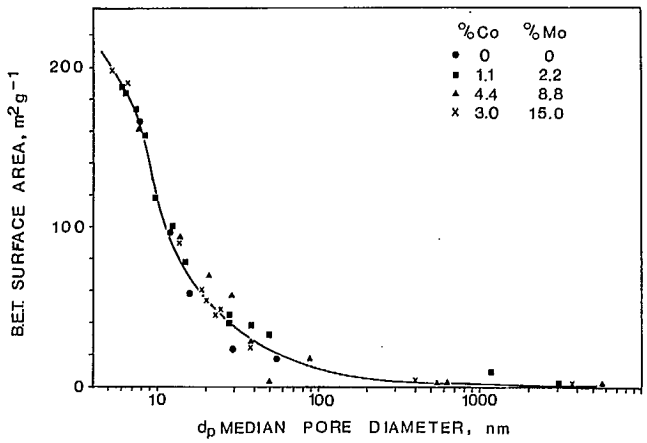

Fig. 3 - Catalyst surface area, m^2/g, versus median pore diameter, nm

creases. This is due to the general increase in extrudate density as d_p increases (Fig. 6 and 7). For catalysts 0.0:0.0 and 1.1:2.2 *m %* CoO: MoO_3, the density increases by only 10% up to 975°C. Above that temperature there is a 25% increase in density. This again corresponds to the transition of lower aluminas - η, γ, Δ, Θ, κ - to corrundum α.

The behaviour of the densities of the 4.4:8.8 Co:Mo Al_2O_3 catalysts follows that described above. However, the turnover to rapid density increase occurs at a lower temperature, i.e., 800°C. This is consistent with the seeding of sintering noted above for surface areas and pore diameters. The presence of cationic impurities is well known to trigger sintering and recrystallization (28).

For catalysts loaded with 3.0:15.0 CoO:MoO_3, the densities do not correlate well with calcination temperature (Fig. 7). The scatter in points and the appearance of many densities for similar calcination temperatures may indicate very large differences in degree of separation of the molybdenum oxide and aluminum oxide phases.

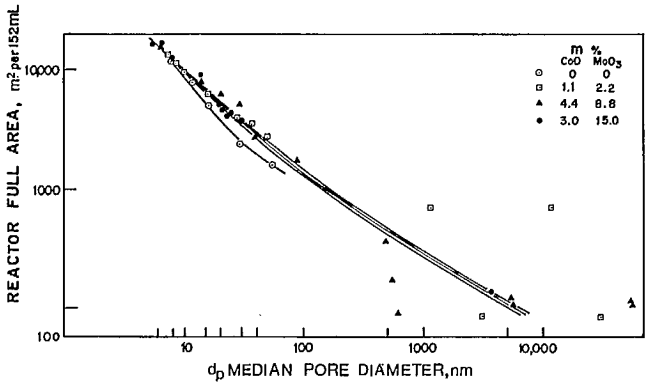

Fig. 4 - Total catalyst surface area in the reactor, m^2, versus median pore diameter, nm

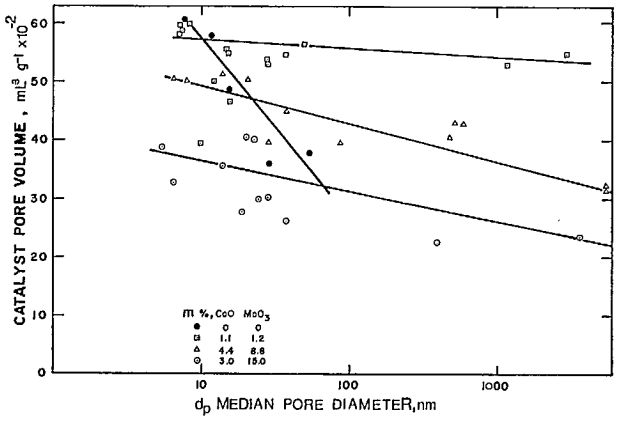

Fig. 5 - Catalyst pore volume, mL/g, versus median pore diameter, nm

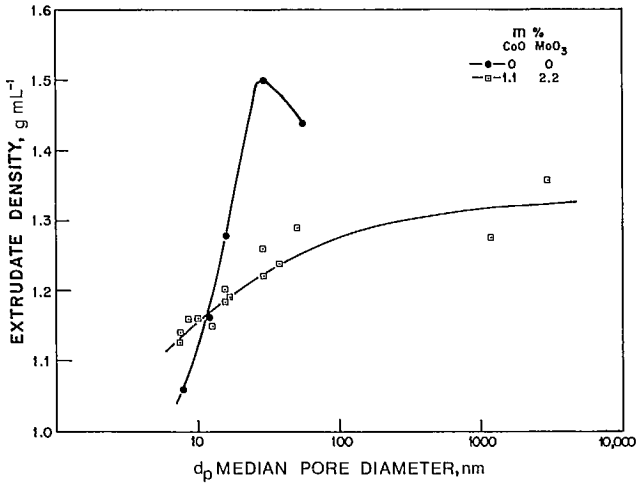

Fig. 6 - Density of catalyst extrudates, g/mL, versus median pore diameter, nm

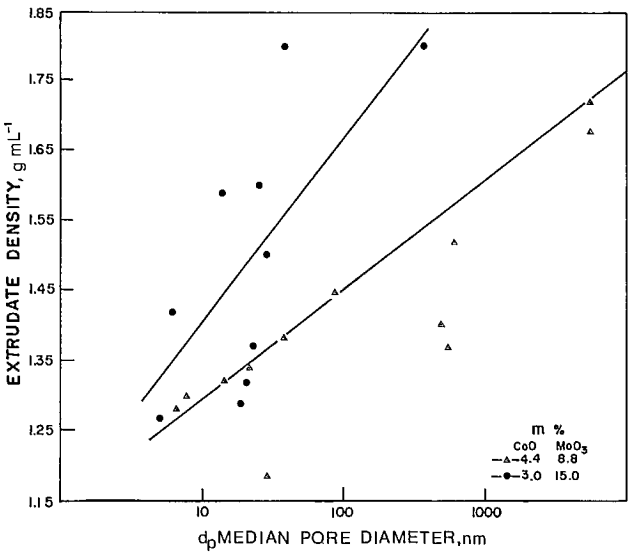

Fig. 7 - Density of catalyst extrudates, g/mL, versus median pore diameter, nm

Bulk chemical analyses of the calcined catalysts were made by atomic absorption spectrophotometry. The elements Co, Mo, and Al were determined and oxygen was taken by difference. It was assumed that in all cases the chemical species were CoO, MoO_3 and Al_2O_3. The results are shown in Fig. 8 and 9 for CoO and MoO_3 respectively.

There is no loss of cobalt as a function of T^C.

In direct contrast, there are significant losses of molybdenum, especially above the calcination temperature above which the aluminas transform to α-Al_2O_3 (Fig. 9). Notice as well that the supposed bare aluminas (0.0:0.0 *m %* CoO:MoO_3) in fact act as getters for molybdenum bdenum subliming from the furnace walls. The ceramic liner of the furnace almost certainly acts as a sink for molybdenum oxides sublimed from other catalysts in prior treatments.

The rapid drop shown in Fig. 9 for the concentration of MoO_3 in 3.0:15.0 catalysts, i.e., above d_p = 30 nm, may not be correct. However, there are no data points between 40 nm and 3700 nm.

The results shown in Fig. 8 and 9 reflect total bulk chemical composition changes. From a catalytic point of view, however, the important factors must be the surface concentrations of cobalt oxide promotor and molybdenum oxide catalyst.

Sublimation of some molybdenum oxide undoubtedly occurred at higher calcining temperatures (31). However, sublimation at pore surfaces may have provided sufficient potential for molybdenum oxide in the bulk to diffuse to the pore surfaces. This replenishment would help to compensate for surface depletion caused by vapourization. As calcining temperature increases, the surface concentration of molybdenum oxide should decrease with increasing pore diameter.

An alternative preparative method would have been to precalcine the support and add the molybdenum and cobalt by solution impregnation. This method would have ensured the same bulk analysis of molybdenum and cobalt for every catalyst. However, the decrease in surface area would cause the surface concentration of molybdenum and cobalt to increase greatly with increasing pore diameter. Therefore solution impregnation is considered inappropriate.

As a surface analysis of the pore walls could not readily be obtained, neither of the above catalyst preparation techniques could be shown to be superior in terms of uniformity of surface concentration. However, the catalyst preparation and calcining method used in this study is likely to cause decreasing surface moly-

bdenum concentration with increasing pore diameter. The following discussion shows that the method used was more appropriate for this study.

Bitumen conversions are clearly going to be affected by all the above factors to some degree. The effects of sintering, pore volume decreases and density increases are demonstrated in

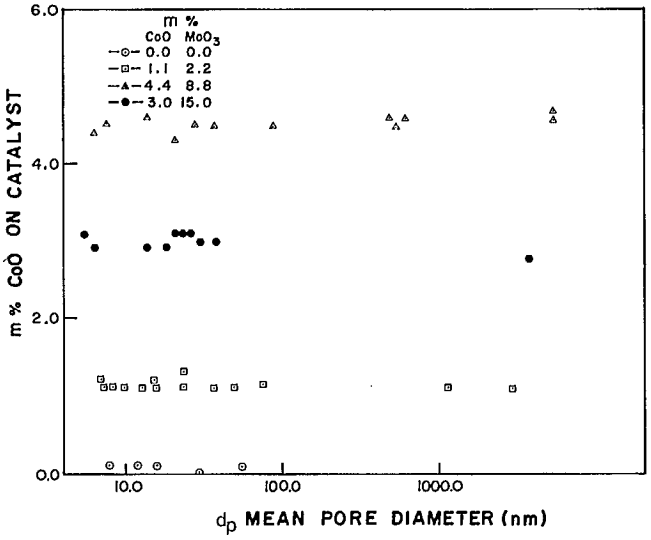

Fig. 8 - Mass per cent CoO on catalyst versus median pore diameter, nm

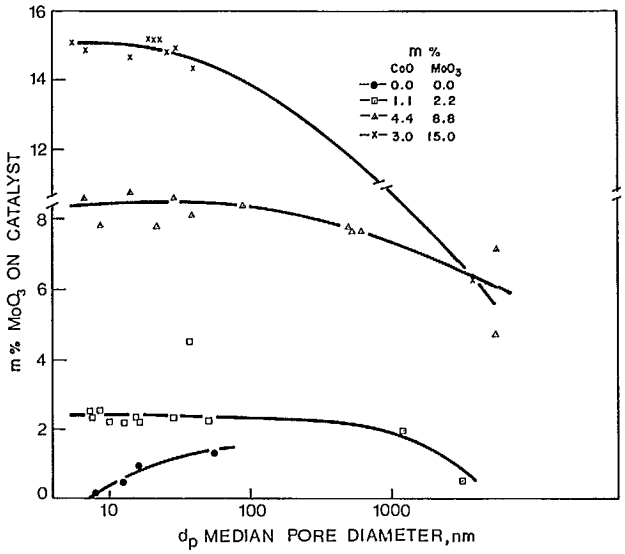

Fig. 9 - Mass per cent MoO_3 on catalyst versus median pore diameter, nm

the number of grams of catalyst loaded into the constant reactor volume (Fig. 10 and 11). As expected, there are sharp increases in the d_p ranges where the transitions from η, γ, Δ, Θ, κ -Al_2O_3 to α-Al_2O_3 begin. However, the sharpest reactor density increases do not correspond to the sharpest increases in extrudate densities (Fig. 6 and 7).

The extrudates varied in length from about 5 mm to 20 mm for any given catalyst. Further, the number density of extrudates having any given length in the range 5-20 mm varied from catalyst to catalyst. Consequently the reactor bulk densities varied due to inhomogeneous packing of extrudates in the reactor. Some of the scatter in the points in Fig. 10 and 11 is due to this. Most of the runs for MB 400 onwards did not have this inhomogeneity. Extrudates having a narrow length distribution range of 8-12 mm were selected.

Finally, the reactor loading curve for catalysts with 4.4:8.8 *m* % CoO:MoO_3 is probably artificially skewed. It is expected that either the points near 500 nm are too low or those near 5000 nm are too high, or both.

CONVERTED BITUMEN PROPERTIES

(a) Relative Densities

Relative densities of the liquid product were measured after equilibration of the samples at ambient conditions for various periods. In general, samples were collected for 1-2 weeks; then the gravities were measured in batches. Consequently the degrees of aging, degassing, and settling were not uniform.

The relative densities, normalized to 288 K and measured to 3 significant figures with hydrometers, are shown in Fig. 12 and 13. The relative density of the feed was 1.009. In comparison, the simulated thermal hydrocracking run, which used 153.2 mL of soft steel having the shape of "extrudates", gave a product with a relative density of 0.960. This reduction from 1.000 to 0.960 is assumed caused by hydrocracking. As well it is assumed that relative density reductions past 0.960 represent some catalytic effect.

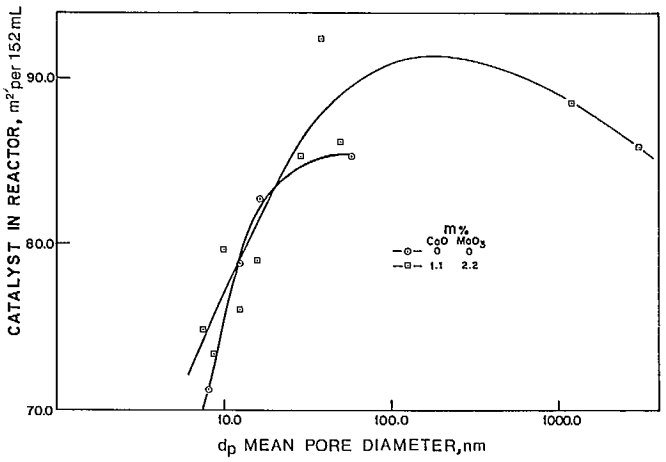

Fig. 10 - Total mass of catalyst in the reactor versus median pore diameter, nm

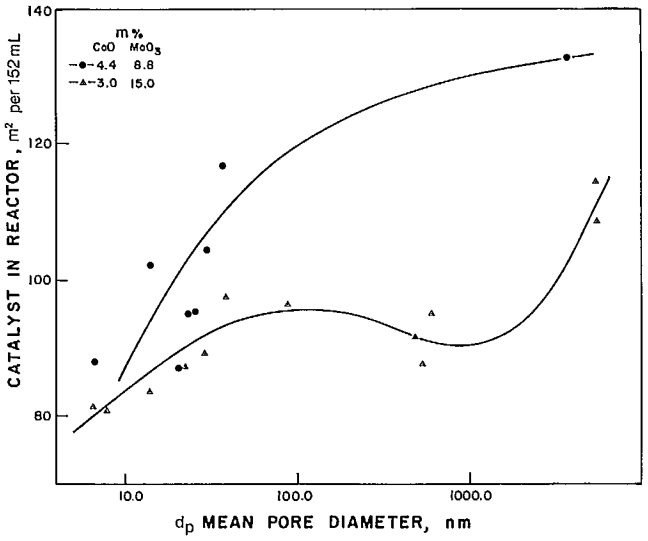

Fig. 11 - Total mass of catalyst in the reactor versus median pore diameter, nm

The relative density of the 0.0:0.0 *m* % catalyst at d_p = 7.4 nm is 0.963, very close to the thermal hydrocracking value (Fig. 12). As expected, the bare alumina support contributes relatively little to hydrogenation and hydrogenolysis (HDS, HDN, HDM), i.e., over and above the thermal effect. Those are the two reaction classes contributing most to liquid product density reductions.

The relatively rapid decrease in relative density for the other 0.0:0.0 $CoMoAl_2O_3$ catalysts follows closely the increase in concentration of molybdenum oxide accumulated during calcination (Fig. 9 and Table 3). The relative densities approach those obtained for the 1.1:2.2 *m* % $CoMoAl_2O_3$ catalysts. In fact, the last three 0.0:0.0 CoMo catalysts have concentrations equivalent to 50% or more of the 2.2 *m* % molybdenum oxides added in the second series (Fig. 9). As well, the accumulated MoO_3 is most probably at, or near, the pore surfaces.

The drop in density obtained with 0.0:0.0 CoMo catalysts as d_p increases is probably mostly due to the hydrogenation and hydrogenolysis caused by high surface concentrations of molybdenum (Fig. 12).

However, increased activity due to increased mass transfer cannot be ruled out even in this case.

Increased mass transfer through increasingly large mean pore diameters did not lead to an apparent decrease in relative density for the 1.1:2.2 *m* % catalysts (Fig. 12). The absence of a minimum relative density as d_p increased may be simply due to the scatter of the experimental data at values of d_p less than 50 nm.

In contrast, the other two series of catalysts, 4.4:8.8 and 3.0:15.0 *m* % $CoMoAl_2O_3$, do show definite minima near d_p = 25 nm ± 10 (Fig. 13). The increase beyond 35 nm can be attributed to rapid losses in surface areas.

Concentrations of added catalyst molybdenum oxide led to regular decreases in relative density of the product as the concentrations increased. The increases follow the concentrations of molybdenum oxides rather than cobalt oxides.

(b) H:C Ratio

The effects of increasing median pore diameters on hydrogenation of the bitumen can be seen in Fig. 14. These must be compared with the feed value of 1.51 and the thermal value of 1.48. Three of the series of catalysts show disinct maxima near d_p = 15 ± 5 nm.

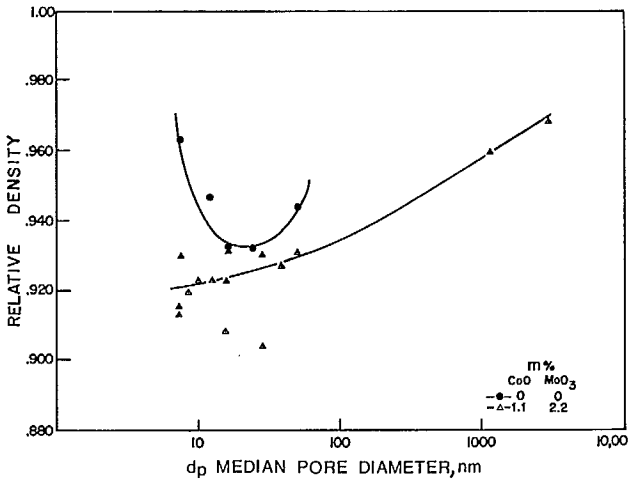

Fig. 12 - Relative density versus median pore diameter, nm

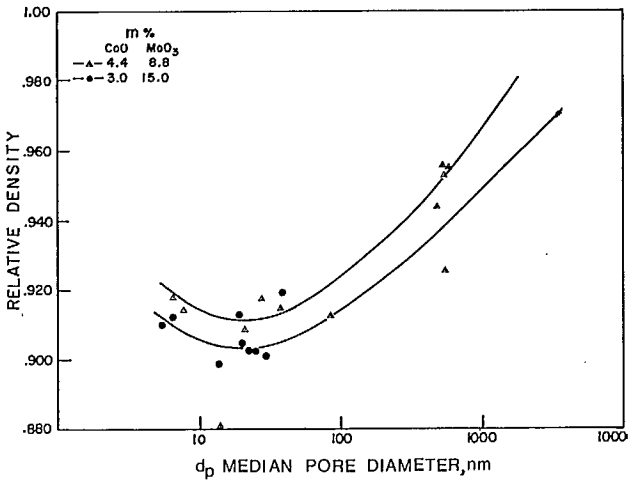

Fig. 13 - Relative density versus median pore diameter, nm

The maximum in hydrogenation activity for the 0.0:0.0 series is probably an artifact of the inadvertent addition of MoO_3 and decreasing surface area.

It is believed the maxima for the H:C ratios produced by 4.4:8.8 and 3.0:15.0 *m* % CoMo Al_2O_3 catalysts reflect real increases in net reaction rate and real decreases in mass transfer limitations.

The increase in the hydrogen to carbon atomic ratio as the pore diameter increases from 7 to 20 nm may be caused by increasing rates of feed and product mass transfer. The decrease in hydrogen to carbon atomic ratio as the pore diameter increases from 20 to 1000 nm may be related to the catalyst surface area. It was shown in Fig. 3 that the catalyst surface area decreased with increasing pore diameter. Thus the decrease in H:C ratio from 20 to 1000 nm may be caused by the decreased number of reaction sites.

(c) Conversion of Pitch and Asphaltenes

Asphaltenes constitute 15 *m* % of the bitumen feed and about 30 *m* % of the +525°C pitch fraction. The asphaltenes are believed to be among the largest in geometric size and molecular mass, at least for those molecular types forming a significant portion of the feed. When precipitated from solution by changes in the ratios of saturates to aromatics to polar compounds - the asphaltenes are believed to form micellular clusters of approximately 1-2 nm.

Species of those sizes are expected to contain relatively high amounts of the total S, N, O and metal heteroatoms, (Table 6) as well as high molecular mass compounds (32). Moieties of 1-2 nm would also be expected to have strong mass transfer limitations in typical commercial catalysts. The latter normally have mean pore diameters in the 5.0-7.0 nm range.

It is apparent then, that conversions of asphaltenes should provide a good measure of variations in mass transfer as d_p increases.

Results for three series of catalysts are shown in Fig. 15. There was 15.0 *m* % asphaltenes - pentane insolubles - in the feed bitumen. The simulated thermal hydrocracking case gave 32.3 *m* % asphaltene removal.

As before, the bare Al_2O_3 support at d_p = 7.2 nm was largely inactive, i.e., the conversion was almost totally thermal. Introduction of small amounts of molybdenum, however, doubled the activity to 62%, near the value for 1.1:2.2 *m* % $CoMoAl_2O_3$ catalysts.

The other two catalyst series shown in Fig. 15, 1.1:2.2 and 3.0:15.0 *m* % metals, show

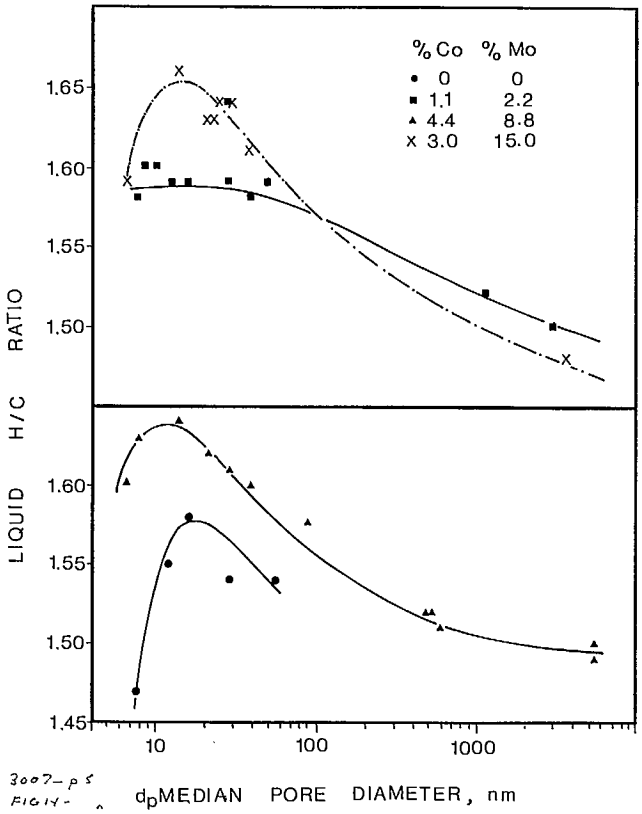

Fig. 14 - Hydrogen to carbon atomic ratio in the liquid product versus median pore diameter, nm

distinct maxima at d_p = 20 ± 10 nm. Over this range of d_p values, the bulk chemical compositions remained relatively constant. It is concluded therefore, that mass transfer limitations do inhibit the net chemical reaction rate for asphaltene conversions.

The maximum in asphaltene conversion as a function of median pore diameter is probably caused by changes in mass transfer limitations and changes in catalyst surface area. The increase in pore size from 7 to 20 nm would allow more rapid mass transfer and might explain the increased asphaltene conversion. The decrease in surface area as the pore diameter increases from 20 to 1000 nm may have caused the decreased asphaltene conversion.

The conversion of asphaltene shown in Fig. 15 is likely related to the changes in hydrogen content of the liquid product shown in Fig. 14. The asphaltenes may be converted to oils and perhaps resin type compounds, both of which generally have higher hydrogen contents and smaller proportions of aromatic structures than asphaltenes. In that case, the higher hydrogen content obtained with the small pore catalysts is consistent with the higher asphaltene conversions. Once again, however, the smaller surface areas present in the large pore catalysts were probably responsible for the lesser extents of reaction.

Concerning pitch conversion at +525°C, there is no consistent trend in the pore size results amongst the four series of catalysts (Fig. 16 and 17). The 0.0:0.0 *m* % metals cat-

Table 6 - Heteroatom concentrations in asphaltenes and total feedstock

	m % in feed	*m* % in asphaltene	*m* % of component in asphaltenes
N	0.35	0.6	25
S	4.5	7.0	23
Ni	90 µg/g	260 µg/g	43
V	300 µg/g	720 µg/g	36
Asphaltenes*	15.0	100	100

*pentane insoluble portion

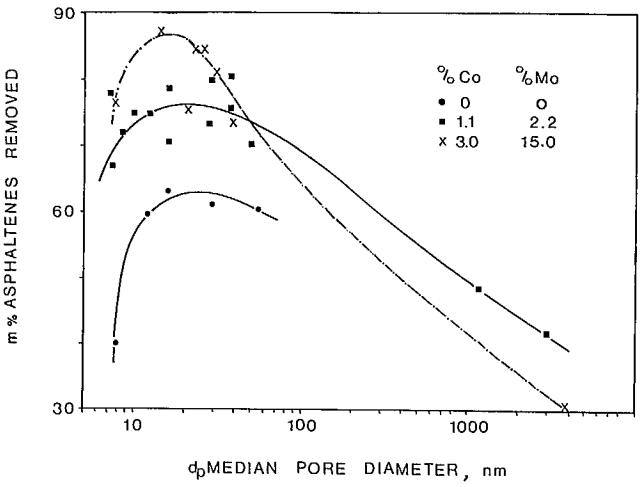

Fig. 15 - Mass per cent asphaltenes removed from the liquid versus median pore diameter, nm

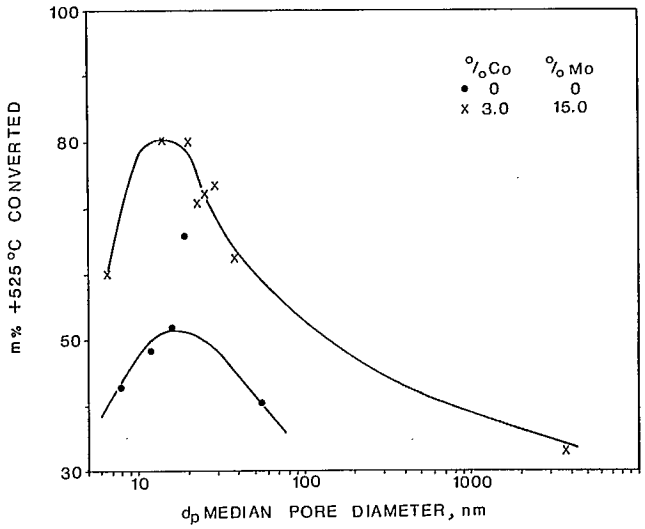

Fig. 16 - Mass per cent +525°C pitch converted versus median pore diameter, nm

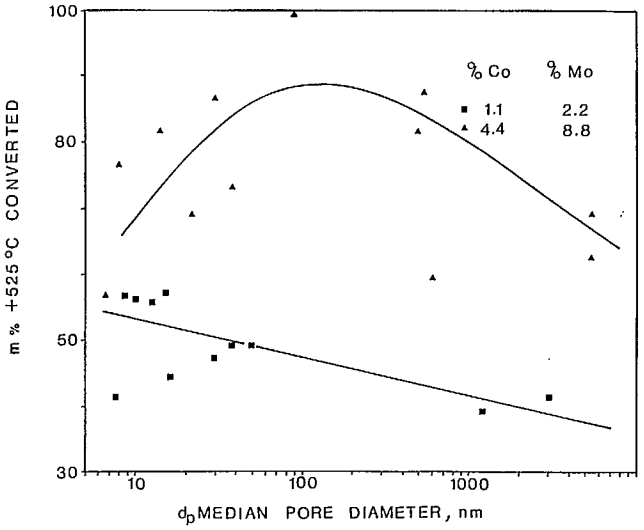

Fig. 17 - Mass per cent +525°C pitch converted versus median pore diameter, nm

alyst rapidly reached 50% conversion, near the values for 1.1:2.2 *m %* catalysts.

However, the shape of this curve differs from previous bare alumina results (Fig. 12 and 13). This might indicate some real, i.e., non-chemical mass transfer pore size effect.

If that is true, it is an interesting result since it indicates there is a chemical reaction in the pores of the bare catalyst support. One normally assumes the support is inactive. However, the electron acceptor centres at Lewis acid sites on the alumina surface may enhance pyrolysis or cracking reactions.

Of the remaining catalyst series only the 3.0:15.0 *m %* series showed a clear maximum, e.g., at d_p = 17 ± 5 nm (Fig. 16). Again the bulk chemical compositions were constant from d_p = 6.0 nm to d_p = 40 nm. This maximum can be attributed to removal of some mass transfer limitations in this catalyst series.

The larger scatter in the data points in Fig. 15 results from errors in distillation.

(d) Aromatics, Olefins and Paraffins

Hydrogenation of aromatics and olefins in the bitumen feed is one of the major hydrogen-consuming reactions. Quantitative analysis of product samples for aromatics, olefins and paraffins has long been problematic. The authors have recently developed a quantitative ^{13}C-^{1}H nmr method for analyzing these molecular types (27). One distinct advantage of the method is that it distinguishes the three types of molecular carbon on an atom-by-atom basis.

The feed and product samples were analyzed after dissolution in CCl_4. Small amounts of mineral matter remained undissolved. The results for all four catalyst series were plotted in Fig. 18 and 19 for the aromatic carbons. Results for paraffinic carbon growth are shown in Fig. 20 and 21.

Analysis of the simulated thermal hydrocracking case gave an aromatic carbon content of 29.7 atomic per cent.

For the 0.0:0.0 *m %* $CoMoAl_2O_3$ catalysts the aromatics content dropped by 4 atomic per cent (Fig. 18).

Alumina is known to be a good isomerization catalyst. The minor amounts of MoO_3 accumulated during calcining might promote hydrogenation reactions. However, the reduction in aromatic atoms may also have been caused by hydrogen transfer reactions during isomerization on the alumina.

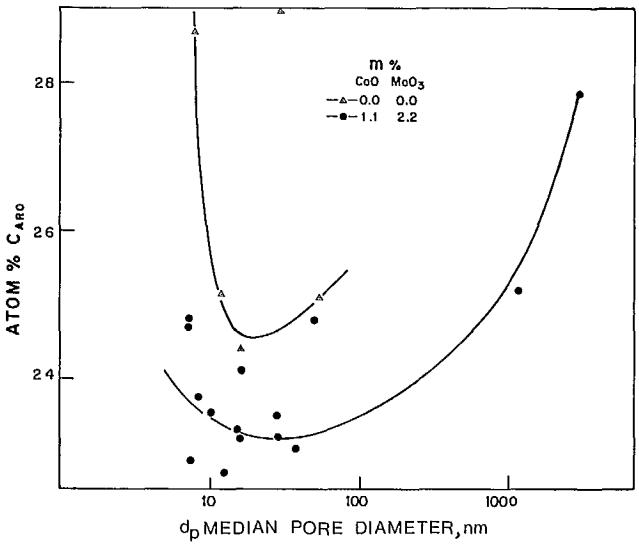

Fig. 18 - Per cent of aromatic carbon atoms in the liquid product versus median pore diameter, nm

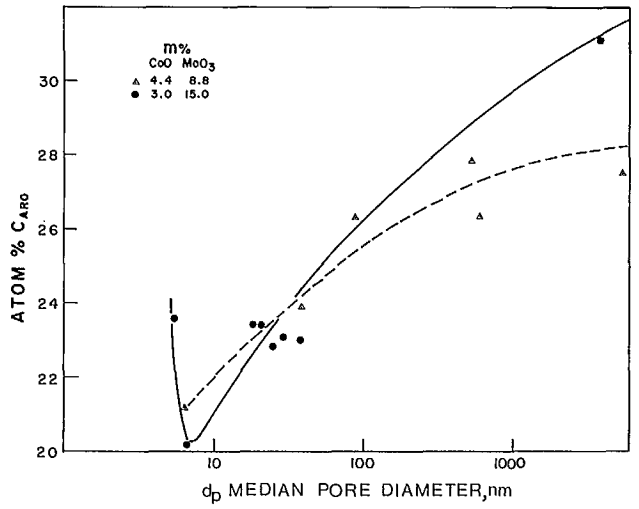

Fig. 19 - Per cent of aromatic carbon atoms in the liquid product versus median pore diameter, nm

Of the remaining three catalyst series, only the 1.1:2.2 *m %* of $CoMoAl_2O_3$ catalysts demonstrated an optimum pore size, e.g., d_p = 27 ± 15 nm in Fig. 16. The other two show apparently steadily increasing aromatics content with no optimum mean pore diameter (Fig. 19). It is possible there is a minimum for the 3.0:15.0 *m %* $CoMoAl_2O_3$ catalysts; however, that seems unlikely in view of the scatter in the data points.

The occurrence of paraffins in the products followed the aromatic trends in a fully complementary manner (Fig. 20 and 21). These should be compared with the thermal value of 69.6 atomic per cent paraffinic carbon atoms.

It is interesting to note that under the reactor conditions used there is remarkably little reduction in the aromatics at 24%, i.e., there is little hydrogenation or ring breaking. That is true irrespective of the amounts of promoter and catalyst present.

The ^{13}C-^{1}H nmr analysis for olefins is less satisfactory as the transitions associated with them overlap with those of the aromatics for ^{13}C analyses. The feed analysis indicated that very little olefinic carbon was present. The thermal case yielded 0.7 atomic per cent olefinic carbon. In contrast, the four series of pore size catalysts gave liquid products containing traces of olefinic carbon, or none at all.

Finally, it is pointed out that these nmr analyses overcome the problem of labelling high molecular mass compounds as aromatics, olefins, or saturates. For example, a molecule having a long paraffin chain attached to an aromatic ring structure, would exhibit properties of both types, especially in HPLC type analyses. The nmr results, however, count atoms in their local environments.

(e) Sulphur and Nitrogen Conversions

Two of the most important reactions occurring during the catalytic hydrocracking of Athabasca bitumen are sulphur and nitrogen hydrogenolysis. The kinetics and mechanisms of these reactions have been studied in detail for pure MoS_2, cobalt-promoted MoS_2, and $CoMoAl_2O_3$ catalysts (33-35). Some general problems relating to residuum HDS, HDM and tar removal were reviewed by Riediger and the conclusions are important considerations for bitumen processing (33). The effects of diffusional limitations in pore systems have been studied to a certain degree (5-11), especially for coal liquid hydrotreating (15).

Beuther et al. (10), Kurito (36), Mosby (37) and others (35) have shown that the HDS reaction appears to be second order up to about 80%

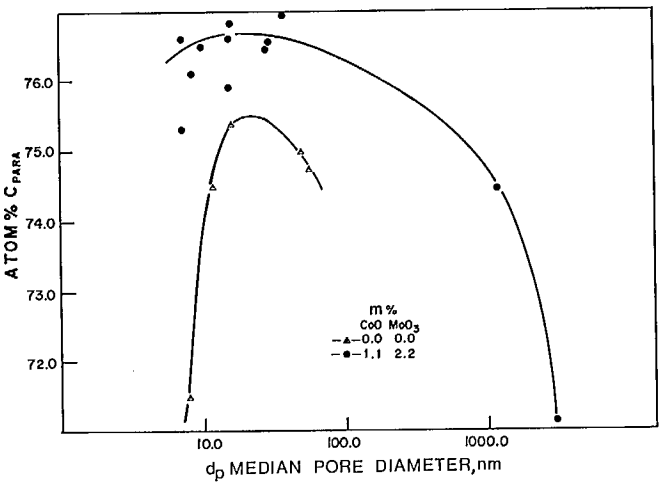

Fig. 20 - Per cent of paraffinic carbon atoms in the liquid product versus median pore diameter, nm

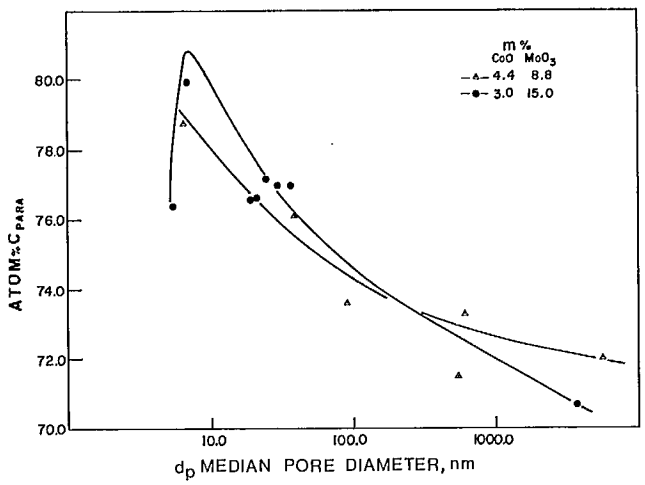

Fig. 21 - Per cent of paraffinic carbon atoms in the liquid product versus median pore diameter, nm

conversion. However, at higher conversions, the feed/product must be broken into four fractions. Each fraction has a first order reaction rate in that case. It is difficult to conceive of a realistic HDS reaction having a bifold sulphur concentration dependence. Rather, the overall pseudo second order rate is believed to be the sum of a large number of increasingly larger first order reaction rates (10). The overall rate can be expressed as (10):

$$\frac{C}{1-C} = k \frac{1}{LHSV} \qquad \text{Eq 1}$$

where k = rate constant and

$$c = 1 - \frac{\text{sulphur in product, } m\,\%}{\text{sulphur in feed, } m\,\%}$$

This equation assumes uniformity of catalyst properties. A more detailed discussion of the reaction rate is given below along with specific reaction rate calculations for four different models. Applying Eq 1 to the data in Fig. 22 and 23 it is seen that the rate constant changes as a function of d_p, even when the surface areas are taken into account (Fig. 3). The implications of this are also discussed below.

As the catalysts vary greatly in area, pore volume and diameters, of more interest is the empirical realtionship given by Beuther and Schmid (10):

$$m\,\%\ \text{HDS} = K + 0.05\%\ A + 13.2\ V + 0.06\ d \qquad \text{Eq 2}$$

where K = constant for severity

A = area, m^2g^{-1}

V = volume pores, mLg^{-1}

d = mean pore diameter, nm

For these experiments it was found there was only one catalyst which gave a clearly defined optimum pore diameter (Fig. 22 and 23). The 4.4:8.8 *m %* catalyst shows a maximum in *m %* sulphur removed at $d_p = 14 \pm 5$ nm. For the 1.1:2.2 *m %* $CoMoAl_2O_3$ catalysts there may be a maximum. For the 3.0:15.0 catalysts there is, at best, a plateau, more probably a negative correlation between *m %* S removed and d_p.

In all further cases the rise in conversion, i.e., *m %* S removed, as d_p increased for the 0.0:0.0 catalysts is attributed to gathered MoO_3. Conversions for these bare catalysts will not be discussed further.

Using Eq 2 one can estimate the severity constant, K, for the series of 4.4:8.8 $CoMoAl_2O_3$ catalysts. As this equation was developed for more normal commercial catalysts with relatively small variations, it might be expected not to apply well here.

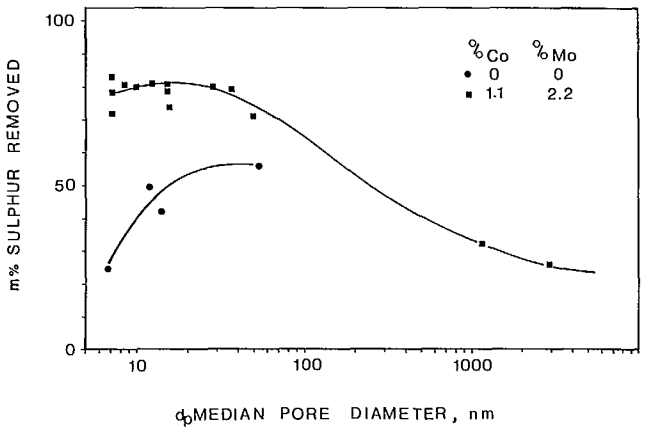

Fig. 22 - Mass per cent sulphur removed from the liquid product versus median pore diameter, nm

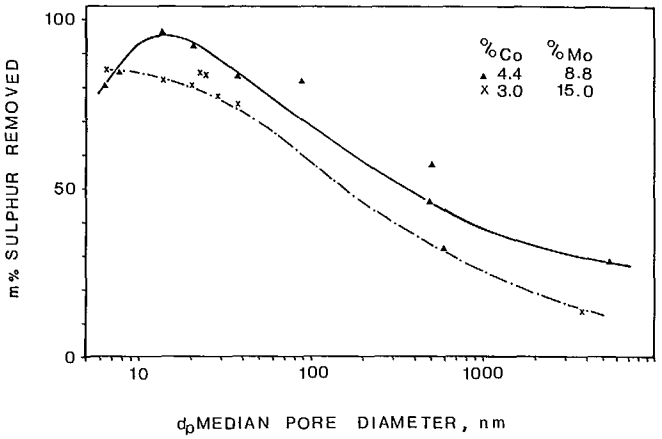

Fig. 23 - Mass per cent sulphur removed from the liquid product versus median pore diameter, nm

Over the range of d_p values where the chemical catalytic moieties on the catalyst are expected to remain more or less constant, i.e., up to about 40 nm, the experimental data show a maximum in net conversion. The values from Eq 2 clearly do not. It would be necessasry to multiply the right hand side of Eq 2 by a constant times a hyperbolic function in d_p to predict the observed behaviour.

The nitrogen in Athabasca bitumen is much more difficult to remove than sulphur. The nitrogen levels in the feed are relatively low at 0.41 *m %* and simulated thermal hydrotreating removed only 12.2 *m %*. It should be noted that the analytical method used for these measurements - microcoulometry - was operating at the lower limits of its practical range. Hence the errors in the data are relatively large (Fig. 24 and 25).

For the two series of low metals CoMo Al_2O_3 catalysts, e.g., 0.0:0.0 and 1.1:2.2, the nitrogen conversions are virtually independent of median pore size d_p. In contrast, the two series of high metals catalysts show distinct

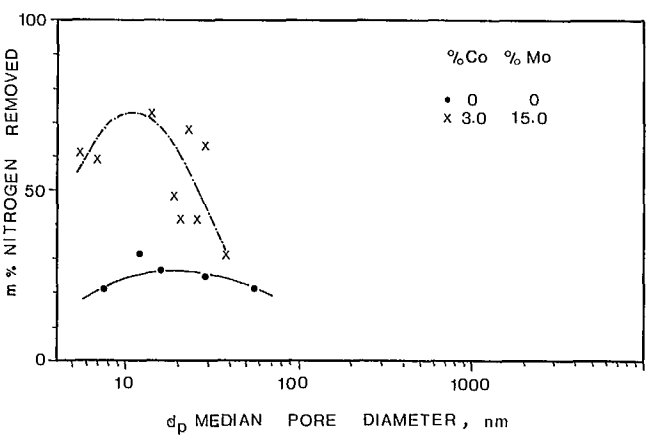

Fig. 24 - Mass per cent nitrogen removed from the liquid product versus median pore diameter, nm

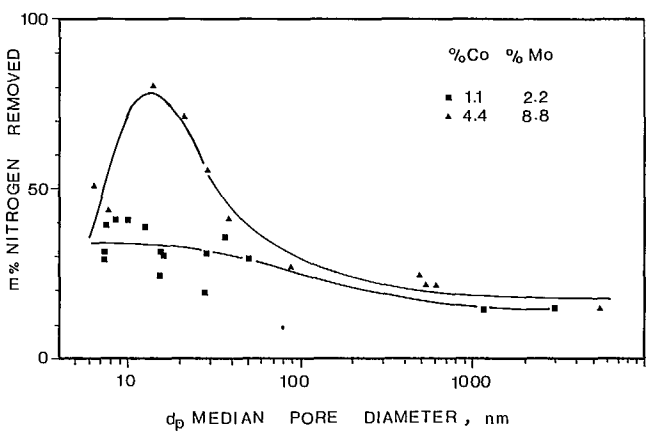

Fig. 25 - Mass per cent nitrogen removed from the liquid product versus median pore diameter, nm

maxima in nitrogen conversion. Between 70 and 80 *m* % nitrogen being removed when the pore sizes were in the range of 12 ± 2 nm and 11 ± 2 nm for 4.4:8.8 and 3.0:15.0 catalysts respectively.

(f) Vanadium, Nickel and Iron Conversions

The very important roles of metals from the feed liquids in catalyst deactivation have been reviewed (10,32,35,38,39). Next to be discussed will be metals deposition on the catalyst. The conversion of metals from the liquid feeds is shown in Fig. 26 and 27 for vanadium, Fig. 28 and 29 for nickel, and Fig. 30 and 31 for iron.

Vanadium is believed to be bound approximately 30% in porphyrins with most of the remainder in the form of cations in salts comple-

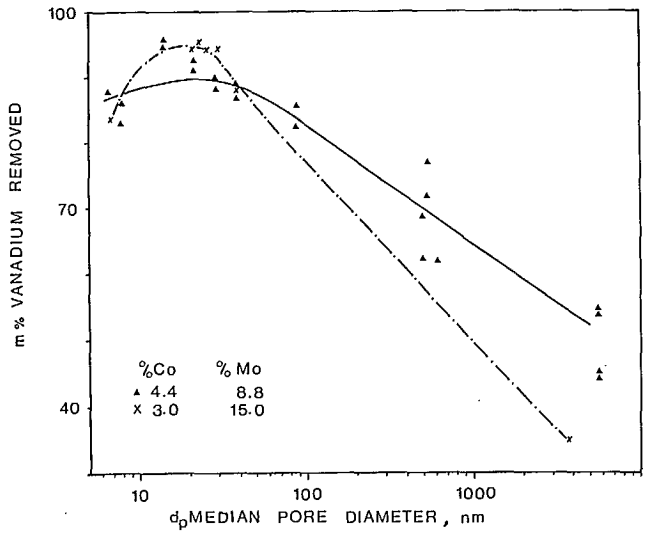

Fig. 26 - Mass per cent vanadium removed from the liquid product versus median pore diameter, nm

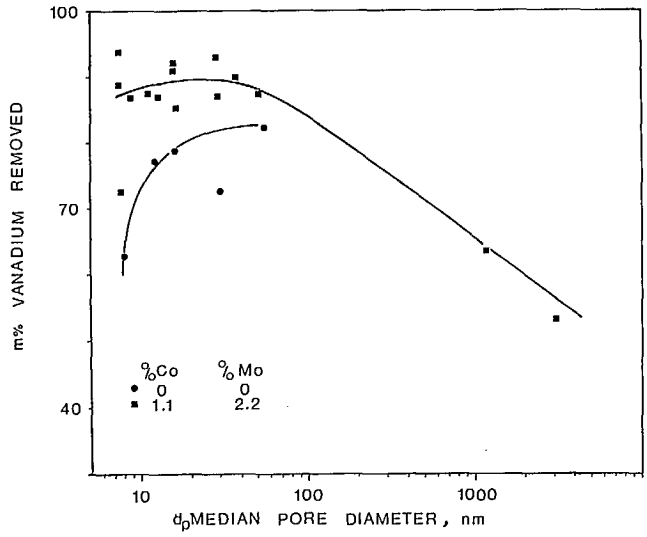

Fig. 27 - Mass per cent vanadium removed from the liquid product versus median pore diameter, nm

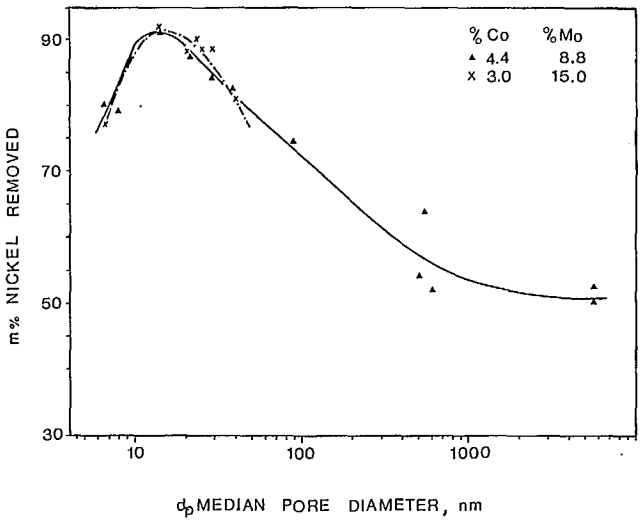

Fig. 28 - Mass per cent nickel removed from the liquid product versus median pore diameter, nm

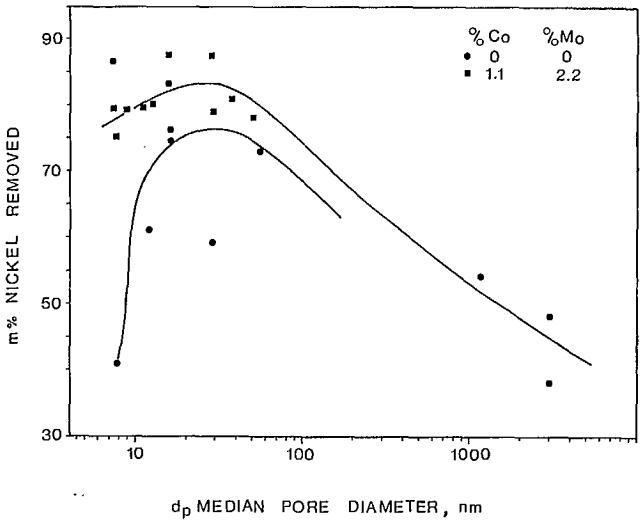

Fig. 29 - Mass per cent nickel removed from the liquid product versus median pore diameter, nm

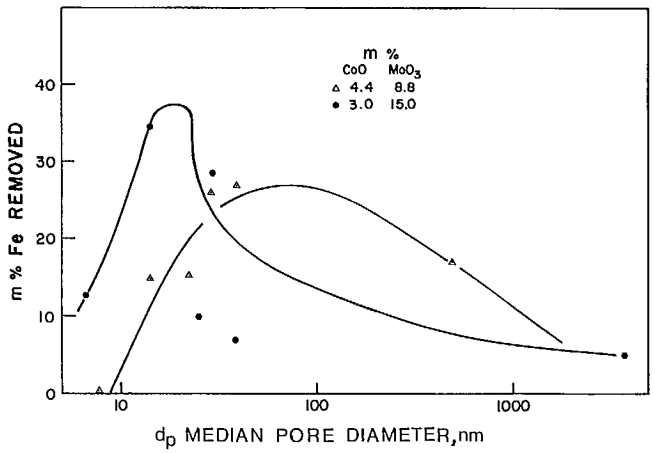

Fig. 30 - Mass per cent iron removed from the liquid product versus median pore diameter, nm

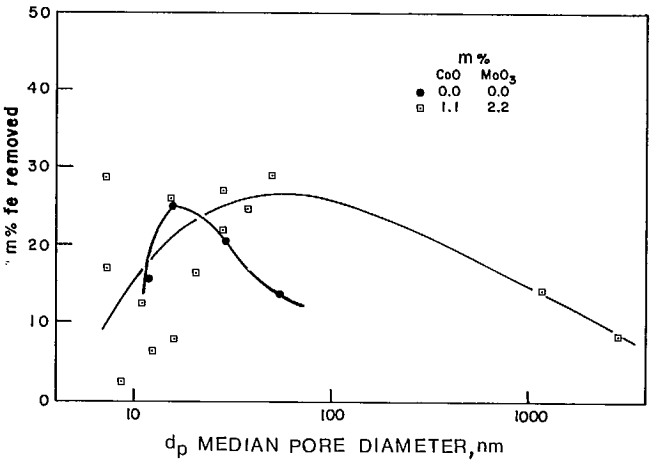

Fig. 31 - Mass per cent iron removed from the liquid product versus median pore diameter, nm

mentary to carbonium ions (40-41). The reaction of demetallization with Lagomedio crude was found to follow second order kinetics for conversions below 83 *m* % (35). For higher conversions, the reaction was found to be first order. The hydrodevanadization (HDV) reaction, in particular, was found to be first order above 83% conversions. The apparent second order behaviour at lower conversions was explained on the basis of many parallel HDM reactions with widely different reaction rates, i.e., one for each molecule or molecule type.

The three catalyst series in this work with Co-Mo promoter-catalyst loadings all show maxima in HDV conversions at d_p = 22 ± 10 nm (Fig. 26 and 27). Two of the catalysts gave only weak maxima, i.e., those with lowest total metals added (1.1:2.2 and 4.4:8.8 *m* % $CoMoO_3$). The maximum vanadium conversions with the former were about 90%, whereas the latter gave up to 95 *m* % vanadium removal. These compare with 24.8 *m* % V removal for thermal hydroprocessing.

The fact that vanadium is indeed easier to remove from the organic complement is clearly demonstrated by the variations in the V:Ni ratio. In the feed the value is 3.4:1. Thermal hydroprocessing yields a product with the total entrained V and Ni decreased, but with ratio constant at 3.4:1. In the catalytically hydroprocessed products, the V:Ni ratio varies from a low of 1.5:1 for small d_p to 2.8:1 for very large d_p. One could conclude that the catalyst lowers the activation energy for the HDV reaction proportionally more than for the hydrodenickelization (HDNi) reaction. This may in part be due to the differences in oxidation state for the V(+4) and Ni(+2) as well as their complexed geometries. Vanadium may interact more strongly with the CoMo Al_2O_3 catalyst through its vacant orbitals than does nickel. As well, vanadium is known to protrude from the mean plane of porphyrin, and is thus less sterically hindered, whereas nickel lies fully in the plane (32,34,35).

Nickel conversions are shown in Fig. 28 and 29 as *m* % Ni removed. The maxima of about 92 *m* % removed are to be compared with thermal values of 25.6 *m* % removed.

The maxima in conversions occur at d_p = 15 ± 5 nm for the 4.4:8.8 and 3.0:15.0 catalysts (Fig. 28). For the 1.1:2.2 catalyst series, the value is somewhat larger, d_p = 25 ± 10 nm, with larger error.

For three series of pore size catalysts, the vanadium removal levels are 5-7 *m* % higher than the nickel removal levels, i.e., for 0.0: 0.0, 1.1:2.2, and 3.0:15.0 *m* % catalysts. This reflects the lowered ease of removal of nickel from petroleum residua in general (32,34,35).

The higher V conversions, compared with nickel, may imply there is not a random distribution of V and Ni between porphyrins and carbonium ion salts. As the carbonium ions are quite reactive and will give up their cations easily, one might deduce there is more V than Ni in the carbonium ion salts. Conversely, the porphyrins could have a higher proportion of Ni, as they are relatively unreactive (34).

Iron in the bitumen feed is believed to be present mainly in entrained mineral matter. This may be due either to particles of Fe_2O_3 from the storage drums or particles of colloidal clay and sand unremoved by the separation process.

Conversions for Fe removal are shown in (Fig. 30 and 31). The thermal conversion level was found to be 32.1 *m %*. With the exception of one experiment, all four catalyst series showed lower Fe conversions than the simulated thermal test.

As well, all four series show maxima as a function of d_p, but they fall in two widely separated ranges (Fig. 30 and 31). The 0.0:0.0 and 3.0:15.0 catalysts show apparent maxima near 18 ± 10 nm. The 1.1:2.2 and 4.4:8.8 *m %* catalysts gave maximum conversions nearer 55 ± 30 nm.

One can conclude there is a real pore size effect, and that it does not only correlate with increased trapping of mineral matter particles in the pores. There is an apparent chemical effect as well.

(g) Catalyst Deposited Metals

The effect of increasing pore size on the penetration of metals deposited on the catalyst from the feed was investigated for the 1.1:2.2 *m %* series. The radial profiles for two used catalysts (d_p = 8.5 nm and 1180 nm) from that series are shown in Fig. 32. The results given show relative microprobe intensities for Fe, Ni and V species, all as a function of radial position in the extrudate. That is to say, as a function of r/R, where r is the radial position of the microprobe and R is the extrudate radius. The catalysts had been de-oiled by benzene soxhlet extraction prior to microprobe analysis.

The results for iron and nickel were somewhat tenuous as the general degree of iron and nickel poisoning (deposition) after only 8 h total reaction time was very low. The average bulk concentrations of Fe and Ni were too small for accurate, rapid microprobe survey scans, i.e., the signal:noise ratios are only about 2:1 or 3:1. The vanadium results were somewhat better, apparently because of the higher deposition rates (34,35).

The iron deposits close to the catalyst outer skin, i.e., at r/R = 1.0. This appeared to be the case independent of pore size (Fig. 32C). Such a result is consistent with the iron being bound in relatively large particles of colloidal clay or other minerals (silicates).

The electron microprobe results for vanadium are more reliable because of the larger

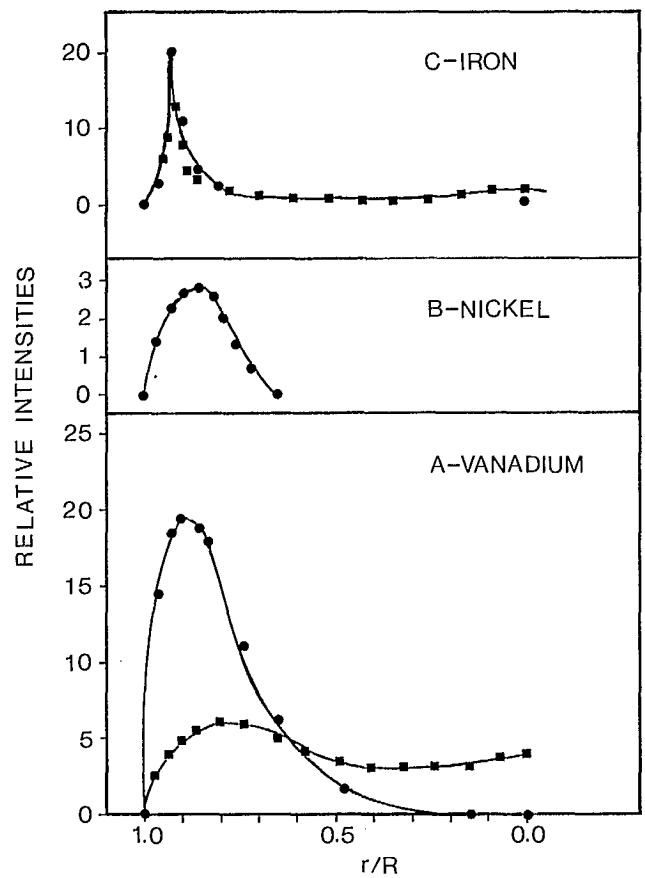

Fig. 32 - Relative intensity or metals concentration (A = vanadium, B = nickel, C = iron) versus radial position in the catalyst extrudate, r/R

concentration of deposited vanadium (Fig. 32A). The profiles for two catalysts, one with small pores at d_p = 8.5 nm and the other with large pores at d_p = 1180 nm, are shown in Fig. 32A. There was a drop in the intensity near the skin as the pores opened. As well, the integrated intensities
from r/R = 1 to r/R = 0 remained relatively constant.

A plot of the position of the peak maximum (r/R for maximum relative peak height) versus mean pore size is given in Fig. 33. This clearly shows the increased penetration of vanadium into the extrudate as the mean pore size increased. However, even at 1180 nm, the maximum is only 22% into the extrudates.

The concentrations of cobalt, molybdenum and sulphur across the extrudates were relatively constant, excluding grain boundary effects. This was true of both new and de-oiled, used catalysts for cobalt and molybdenum.

(h) Catalyst Coke Compositions

Used catalysts were de-oiled by benzene soxhlet extraction and thermal solvent evaporation

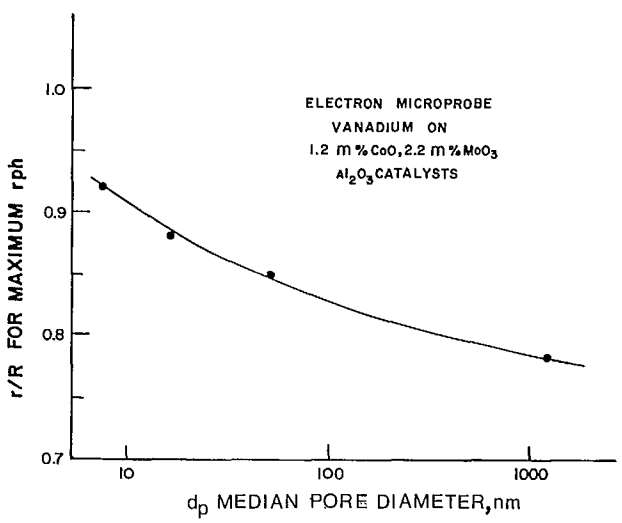

Fig. 33 - Radial position, r/R, in the catalyst having maximum vanadium deposition, maximum relative peak height, rph, versus median pore diameter, nm

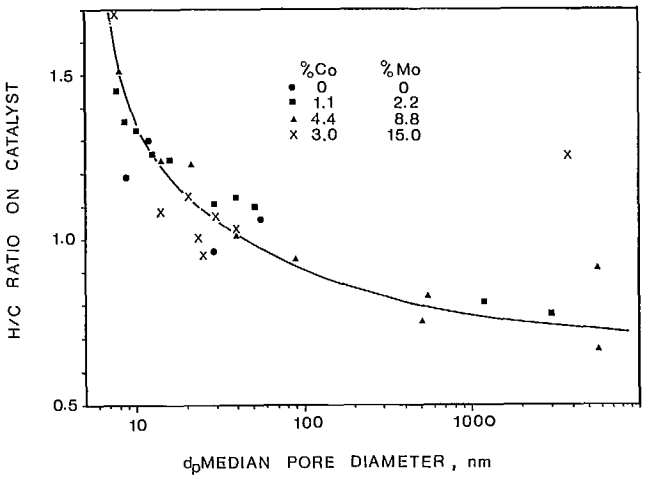

Fig. 34 - Atomic hydrogen to carbon ratio of coke in used catalyst versus median pore diameter, nm

in air. The used, de-oiled catalysts were analyzed for C, N and H.

The H:C ratios for the coke remaining on the catalysts are shown in Fig. 34 as a function of increasing median pore diameters. It is interesting to note that the H:C ratios change in a manner apparently unrelated to catalyst and promoter loadings. This may be due to coke saturation due to the relatively long reaction times with respect to coke formation. Qader et al. have shown that the rate of coke formation drops drastically after 120 min for hydroprocessing heavy cycle oil in a system similar to the authors' but using a $NiWS_2SiO_2Al_2O_3$ catalyst (43).

An alternative explanation may be given. Large reactive molecules, with net reaction rate limited by mass transfer inhibitions, can progressively contribute more to the coke layers as d_p increases and the inhibitions decrease. If the molecules in this inhibited fraction have low H:C ratios, then the observed decrease in H:C ratio of catalyst coke could be explained.

In general terms, Fig. 34 can be divided into three regions: < 20 nm, 20-100 nm and 100-5000 nm. In the first, the H:C ratio corresponds to coke having a mixture of CH and CH_2 groups, mostly aromatic or conjugated, chain unsaturates with some added saturates. Region two corres-

ponds, on average to a relatively simple aromatic system and region three would appear to be a system of condensed aromatic rings. Such a system has been suggested before, and a good analysis of coke on catalysts used for processing reduced crudes was given by Katsobashvili and Nechaev (44).

However, it is important to distinguish between coke precursors and coke constituents. Beuther has shown that for Kuwait residuum the coke formation is decreased by removing the asphaltenes (10). He proposed that coke is formed from large, highly reactive molecules which undergo uncontrolled cracking. On a comparative basis, 6-member aromatic ring structures are relatively stable. Conjugated chains and carbonium ions react more easily.

Although catalyst coke resembles asphaltenes in some ways, it is not correct to assume one transforms to the other. The end product of unknown reactants yields an asphaltene-like structure.

The catalyst carbon content and catalyst nitrogen content are shown in Fig. 35 and 36 respectively. Each quantity is expressed on a unit surface area basis. With the equipment used in this study it was not possible to accurately determine low values of surface areas in catalysts. Those catalysts having very low surface areas - that is catalysts whose median pore diameters were greater than 100 nm (Table A-1) - have not been represented in Fig. 35 and 36.

The data for catalyst carbon content in Fig. 35 are somewhat scattered. The straight line through the data has a correlation coefficient of 0.78. The figure indicates that as the catalyst pores become larger, more coke is deposited per unit surface area. Physically this means that the larger pores provide access for larger molecules. The proportion of condensed aromatic rings probably increases with molecular size. This will decrease their hydrogen content and should increase the possibility of coke formation during cracking.

For pore sizes smaller than 8 nm there is a decrease in carbon content with increasing concentration of molybdenum and cobalt on the catalyst. This result is consistent with earlier findings obtained using a gas oil feedstock, rather than the bitumen feedstock used in this study (45). However, in general there does not appear to be any relationship between the chemical

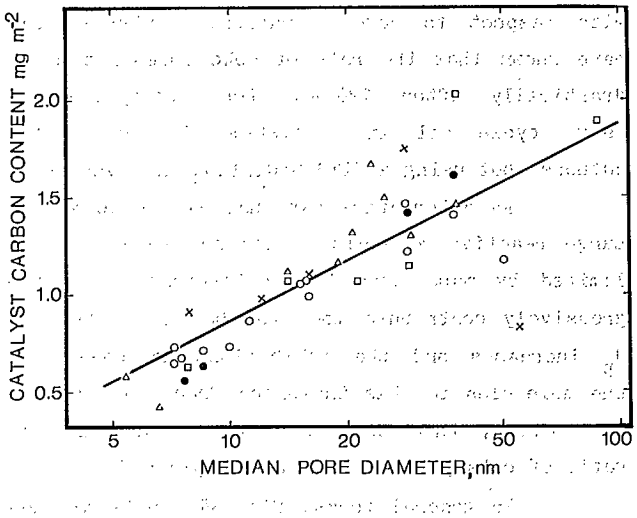

Fig. 35 - Amount of carbon on the used catalyst, mg/m^2, versus median pore diameter, nm. Crosses, circles, squares and triangles represent catalyst containing 0.0:0.0, 2.2:1.1, 8.8:4.4, and 15.0:3.0 *m* % MoO_3:CoO respectively.

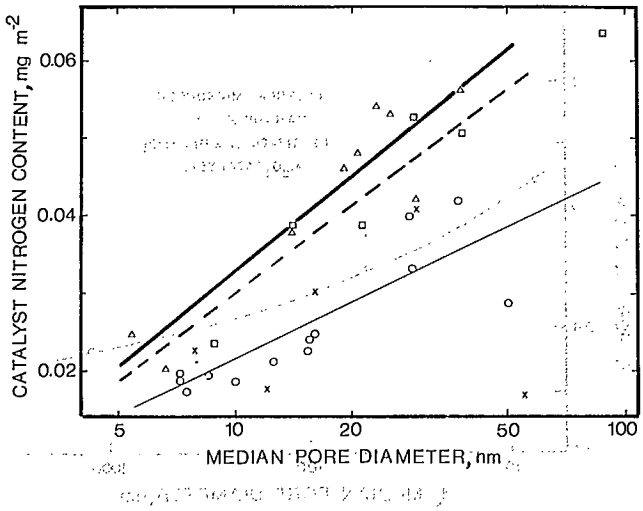

Fig. 36 - Amount of nitrogen on the used catalyst, mg/m^2, versus median pore diameter, nm. Crosses, circles, squares and triangles represent 0.0:0.0, 2.2:1.1, 8.8:4.4, and 15.0:3.0 *m* % MoO_3:CoO respectively.

composition of the catalyst and its carbon content.

The catalyst nitrogen content shown in Fig. 36 also increases with increasing pore size. As the carbonaceous deposits also contain nitrogen, one would expect the nitrogen content to increase with increasing carbon content. There does seem to be a relationship between the catalyst nitrogen content and the amount of molybdenum and cobalt compounds in the catalyst. The three lines in Fig. 36 have correlation coefficients of 0.92, 0.96 and 0.86 for 15:3, 8.8:4.4, and 2.2:1.1 *m* % MoO_3:CoO on the catalyst. It is likely that nitrogen atoms in the hydrocarbon molecules are strongly absorbed by molybdenum atoms in the catalyst. Figure 36 supports this in that the catalysts with the greatest molybdenum content are the ones having the highest deposited nitrogen. The data points for the catalysts not containing any molybdenum or cobalt do not fit this pattern.

THE INFLUENCE OF DIFFUSION ON REACTION RATES

(a) Combined Effect of Pore Size and Surface Area on Diffusion

One reason for developing catalysts with larger pores is to permit rapid diffusion of the large molecules and asphaltene micelles in bitumen. Such pore size effects have been studied previously in this laboratory (46,47,48). The rate of reaction in catalysts having conventional pore sizes is limited by the rate at which the bitumen can diffuse to the reactive site. Therefore, increasing the catalyst pore size would be expected to increase the reaction rate.

This expectation is only partially verified by the conversion data in this report. For example, Fig. 15 indicates an increase in reaction as the pore size is increased up to about 15 nm. However, virtually all the conversion data show a decrease in reaction as the pore size increases beyond 50 nm.

There is a simple explanation for decreasing conversion with increasing pore size. As the pore size increases, the catalyst surface area decreases. This phenomenon is shown in Fig. 3. As the catalyst surface area decreases, the number of reactive sites also decreases. In an attempt to isolate the surface area effect from the pore size effect, reaction rates have been calculated on a unit surface area basis.

(b) Basis of Calculation

The units chosen for the reaction rate are similar to those of a turnover number. The exact units used are number of heteroatoms - S or N - removed per unit time in ks per unit of surface area in nm^2. Desulphurization and denitrogenation proceed by thermal and catalytic mechanisms simultaneously. The amount of reaction occurring thermally was subtracted from the total reaction measured experimentally before calculating the catalytic reaction rate. The thermal reaction was measured by filling the reactor with stainless steel cylinders having the same dimensions as the catalyst particles. The results from the experiment are reported in Table A-2 along with results from experiments in which catalysts were used.

Reaction rates were calculated for the three sets of catalysts containing 2.2:1.1, 8.8:4.4, and 15.0:3.0 *m* % MoO_3:CoO respectively. The set of catalysts which were intended to contain only alumina, were contaminated in the calcining stage. The amounts of MoO_3 and CoO which they accumulated, complicated the interpretation of the reaction results (Table A-1). Therefore they were excluded from the set of calculations currently being discussed.

The total catalyst surface area in the reactor, shown in Fig. 37, was calculated from the catalyst surface area in m^2/g and the amount of catalyst loaded into the reactor. The data in Appendix A indicate that both of these quantities vary considerably. In spite of these variations the solid line in Fig. 37 represents all three families of catalysts for pore sizes less than 100 nm and has a correlation coefficient of -0.97. Unfortunately the equipment available was not capable of obtaining accurate results on solids of very low surface areas. This inaccuracy is responsible for the data scatter in catalysts with pore diameters greater than 100 nm, as shown

in Fig. 37. Appendix A, Table A-1 shows some surface areas reported as "less than values". These results were not included in Fig. 37. The dotted line is an extrapolation into the region of inaccurate surface area determination.

In calculating the reaction rates for catalytic desulphurization, shown in Fig. 38, and for catalytic denitrogenation, shown in Fig. 39, the measured values for total surface area were used for catalysts having pore diameters less than 100 nm. For catalysts having pore diameters greater than 100 nm, surface area values were taken from the dotted line in Fig. 37. For the catalysts having very low surface areas, the total reaction barely exceeded the thermal reaction. Therefore those results for which the catalytic sulphur or nitrogen removal was not at least 5% of the corresponding thermal value, were excluded from Fig. 38 and 39. When two numbers of almost the same value are subtracted, the errors in the result become large. By excluding these data points which potentially have large errors, data scatter in Fig. 38 and 39 was reduced.

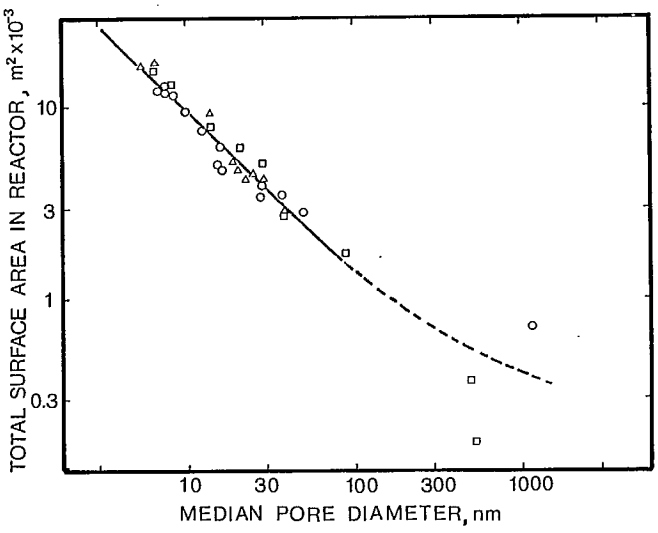

Fig. 37 - Total surface area in reactor, m^2, versus median pore diameter, nm. Circles, squares and triangles represent 2.2:1.1, 8.8: 4.4, and 15.0:3.0 *m* % MoO_3:CoO respectively.

(c) Sulphur Removal

The data on sulphur removal in Fig. 38 can be placed in two groups. For pore diameters less than 50 nm, all the data for all catalyst series are grouped around the same solid line. For example, the molybdenum content of the catalyst series varied from 2.2 to 15 *m* %. This variation did not affect the reaction results. It indicates that reaction rate was controlled by the rate of diffusion rather than by the concentration of catalytic species on the support. Furthermore, Fig. 38 indicates that the diffusion rate controls the reaction rate for all catalysts having pore diameters less than 50 nm.

The second group of data is for those catalysts having pore diameters larger than 50 nm. The dotted lines in Fig. 38 have been drawn with no change in reaction rate with increasing pore diameter. This means that the rate of diffusion does not control the reaction rate. For the very large pore catalysts the overall reaction rate is probably controlled by the intrinsic rate on the surface. Figure 38 shows that the catalytic desulphurization rate reaches a maximum of 6 S atoms removed $(ks)^{-1}(nm)^{-2}$ for the catalysts containing 2.2 *m* % MoO_3 and 1.1 *m* % CoO. The maximum rate for the catalyst series containing 8.8 *m* % MoO_3 and 4.4 *m* % CoO was drawn as 16.6 S atoms removed $(ks)^{-1}(nm)^{-2}$. Of the data points in Fig. 38 representing catalysts containing 15 *m* % MoO_3 and 3 *m* % CoO, none had pores sufficiently large not to have diffusion effects. If sufficiently large pore catalysts containing 15 *m* % MoO_3 and 3 *m* % CoO had been represented in Fig. 38, it is expected that the maximum reaction rate for these catalysts would have been greater than for either of the other two series. Thus, the greater the concentration of catalytic material MoO_3 and CoO on the catalyst the greater the reaction rate when diffusion effects were absent. However, as mentioned previously when diffusion effects were present, similar reaction rates were obtained for all catalysts regardless of the concentration of catalytic ingredients.

(d) Nitrogen Removal

The data for nitrogen removal shown in Fig. 39 follow the same trends as that for sulphur

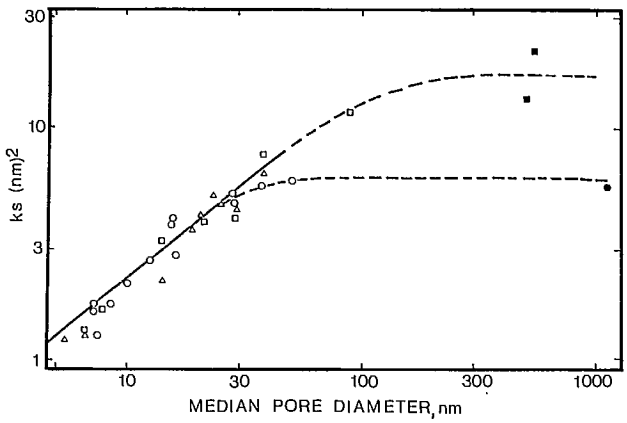

Fig. 38 - Atoms sulphur removed per unit surface area per unit time, atom S ks^{-1} nm^{-2}, versus median pore diameter, nm. Circles, squares and triangles represent catalysts containing 2.2:1.1, 8.8:4.4 and 15.0:3.0 *m* % MoO_3:CoO respectively.

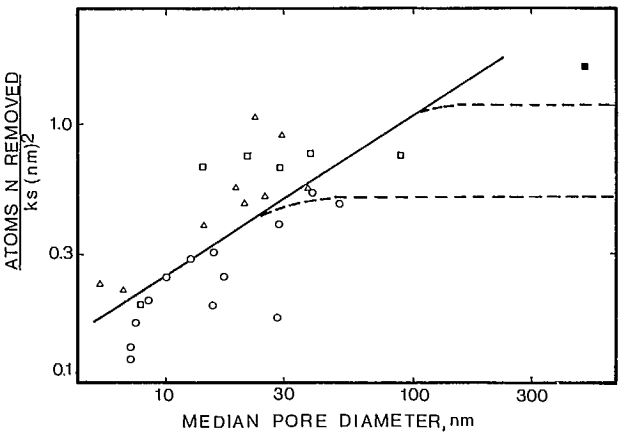

Fig. 39 - Atoms nitrogen removed per unit surface area per unit time, atoms N ks^{-1} nm^{-2}, versus median pore diameter, nm. Circles, squares and triangles represent catalysts containing 2.2:1.1, 8.8:4.4 and 15.0:3.0 *m* % MoO_3:CoO respectively.

removal shown in Fig. 38. However, the nitrogen data are much more scattered. There has often been difficulty in obtaining accurate and reproducible nitrogen analysis on samples produced in the CANMET laboratory. The difficulty may be related to non-homogeneous samples or to the equipment used for nitrogen analysis.

In spite of the scatter, the nitrogen data in Fig. 39 suggest that the catalytic reaction rate is controlled by diffusion for catalyst pore sizes below 50 nm. Dotted lines have been drawn to represent diffusion-free reaction rates. However, the exact location is less certain for nitrogen than for sulphur. The dotted lines indicate that diffusion-free reaction rates of 5 and 12 N atoms removed per ks per $(nm)^2$ were attained by the catalyst series containing 2.2:1.1 and 8.8:4.4 *m* % MoO_3/CoO respectively.

(e) Diffusion Coefficients and Effectiveness Factors

Effective diffusion coefficients can be calculated from the data in Fig. 38 and 39. The following theoretical development indicates how diffusion coefficients and effectiveness factors can be calculated.

The effectiveness factor, η, is the diffusion controlled rate of reaction, r_D which is measured, divided by the diffusion-free reaction rate, r_{DF}. For large values of the Thiele modules, ϕ, η can be written as:

$$\eta = \frac{1}{\phi} \qquad \text{Eq 3}$$

where

$$\phi = L \sqrt{\frac{4\, k_s}{d_p\, D_{eff}}} \qquad \text{Eq 4}$$

L and d_p are the pore length and pore diameter, k_s is the intrinsic reaction rate constant per unit surface area of catalyst, and D_{eff} is the effective diffusion coefficient. For the purposes of this discussion the effective diffusion coefficient will be assumed to be a function of the pore diameter. Thus:

$$D_{eff} = (d_p)^m\, G \qquad \text{Eq 5}$$

where m is a constant and G is a function which is independent of the pore diameter.

Equations 3, 4 and 5 can be combined to obtain

$$\eta = \frac{r_D}{r_{DF}} = C\, d_p^{(m+1)/2} \qquad \text{Eq 6}$$

where $$C = \sqrt{\frac{G}{4\ k_s\ L^2}}$$ Eq 7

Equation 6 can be expressed in terms of logarithms as

$$\ln r_D = (m + 1)/2 \ln d_p + \ln (Cr_{DF})$$ Eq 8

Equation 8 shows that the slope of the line relating $\ln r_D$ and $\ln d_p$ will be equal to $(m + 1)/2$. Figures 38 and 39 produced slopes of 0.82 and 0.65 and m values of 0.63 and 0.3 respectively.

This analysis definitely shows that the diffusion coefficients are a function of the pore diameter. Desulphurization and denitrogenation may have different diffusion coefficients for several reasons. One may be that the nitrogen heteroatoms are contained in different types of molecular species than sulphur heteroatoms. Figures 38 and 39 can also be used to calculate effectiveness factors. The horizontal dotted lines represent the diffusion-free reaction rates. For desulphurization, effectiveness factors for the 2.2:1.1 catalysts vary from 0.22 to 1 and for the 8.8:4.4 catalysts from 0.08 to 1. For denitrogenation, effectiveness factors vary from 0.22 to 1 for the 2.2:1.1 catalysts and from 0.16 to 1 for the 8.8:4.4 catalysts. The range of effectiveness factors found here spans the range of values reported in the literature by Shah and Paraskos (49).

CONCLUSIONS

This work has demonstrated that the conversion of bitumen is limited by the rate of mass transfer in small pore catalysts. Increasing the catalyst pore size was found to increase the catalyst effectiveness factor significantly.

The low effectiveness factors of approximately 0.2, when hydrocracking bitumen with conventional catalysts indicate the need for better catalysts. The development of catalysts having both larger pore diameters and high surface areas is obviously essential.

Another potential problem is related to the greater amount of coke deposited per unit of surface area on the large pore catalysts, as described in the previous section on catalyst coke composition. The effect of increased coke deposition will have to be investigated by long-term catalyst life testing. As the hydrogen to carbon ratio in the coke decreases with increasing pore size, the possibility of the coke being hydrogenated and leaving the catalyst surface diminishes. Both the greater quantity of coke and the lower hydrogen to carbon ratio suggest that large pore catalysts might have shorter useful lifetimes.

An advantageous feature of large pore catalysts is the increased dispersion of metals which foul the catalyst. Figure 32 shows that with small pore catalysts vanadium is deposited predominantly at the exterior surface of the extruded catalyst particle. As the pore diameter increases, vanadium tends to be dispersed more evenly throughout the catalyst. Because the deposition of metals decreases catalyst life, spreading the metals throughout the catalyst is desirable. In catalysts with small diameter pores, because of mass transfer limitations, the exterior of the extrudate is the region most likely to catalyze a reaction. It is also the region most likely to be fouled by metals. By increasing the pore diameter, mass transfer limitations are decreased and the metals are spread more evenly throughout the catalyst. This means that fewer metal atoms are deposited per unit area and the catalyst life will be extended.

ACKNOWLEDGEMENTS

The authors would like to acknowledge the contributions of M. Fulton for performing the bulk of the experimental work and R. Ozubko for making the C^{13} nmr measurements.

REFERENCES

1. Backman, W.A. and Stormont, D.H. "Athabasca ready to yield its hydrocarbons"; Oil and Gas J; Oct. 23, 1969; 1967.

2. Gray, G.R. "Conversion of Athabasca bitumen"; Amer Inst Chem Eng, 71st Nat Meet, Symposium Series 69N127:199, 1972; Dallas; Feb. 20-23, 1972.

3. Hardin, A.H. "Catalytic hydrocracking of residuums via the H-Oil process"; Division Report ERP/ERL 79-50; CANMET, Energy, Mines and Resources Canada; 1979.

4. Hardin, A.H., Pruden, B.P. and Denis, J.M. "Evaluation of the L-C fining commercial hydrocracking unit at Salemanca, Mexico"; Division Report ERP/ERL 78-35; CANMET, Energy, Mines and Resources Canada; 1978.

5. Cuenca, A., Galiasso, R. and Andreu, P. "Development of hydrodesulphurization and hydrodemetallization catalysts for treating heavy oils"; Proc Second Pacific Chem Eng Congress; Denver; 2:1:562; 1977.

6. Hardin, A.H., Packwood, R., and Ternan, M. "Effects of median pore diameters in Co/Mo Al_2O_3 catalysts on the conversion of bitumen"; Am Chem Soc, Div Petrol Chem, Prepr; Miami; 23:4:1450; 1978.

7. Ahmed, M.M. and Crynes, B.L. "Coal liquids hydrotreatment - catalyst pore size effects"; Am Chem Soc, Petrol Chem, Prepr; Miami; 23:4: 1377; 1978.

8. Frayer, J.A., Stauffer, H.C., Wynne, F.E. and Yanik, S.J. "Combination residual oil hydrodesulphurization and thermal cracking process"; U.S. Patent; 4,179,355; 1979.

9. Van Zoonen, D. "Effect of pellet structure on catalyst performance in the hydrodesulphurization of straight-run gas oil"; J Inst Pet; London; 49:383; 1963.

10. Beuther, H. and Schmid, B.K. "Reaction mechanisms and rates in residue hydrodesulphurization"; Proc Sixth World Pet Congress; Frankfurt; III:20:297; 1963.

11. Galiasso, R., Andreu, P., Carrasquel, R. and Petit, R. "Kinetics of hydrodesulphurization and hydrodemetallization catalyst regeneration"; Chem Inst Canada, Sixth Can Symp Catalysis, Prepr; Ottawa; 6:184; 1979.

12. Parsons, B.I. and McColgan, E.C. "The hydrocracking of residual oils and tars - Part 6. Catalyst deactivation by coke and metals deposition"; Mines Branch Report R273; CANMET, Energy, Mines and Resources Canada; 1977.

13. Speight, J.G. "Skeletal structures of petroleum heavy ends"; Proc Nat Sci Workshop on Coal; Knoxville, Tennessee; 125; 1975.

14. Hardin, A. Unpublished data; 1977.

15. Bertolacini, R.J., Gutberlet, E.C., Kim, D.K. and Robinson, K.K. "Relation of coal liquefaction catalyst properties to performance"; Am Chem Soc Prepr Div Fuel Chem; 231:1; 1978.

16. Kang, C.C. and Gendler, J. "Effect of catalyst pore size distribution upon hydrodenitrogenation of heavy coal liquids"; Am Petrol Soc, Div Petrol Chem, Prepr; 23:4:1412; 1978.

17. Richardson, R.L. and Alley, S.K. "Consideration of catalyst pore structure and asphal-

tenic sulphur in the hydrodesulphurization of resids"; Am Chem Soc Symposium Series; 20: 136; 1975.

18. Zautiva, A. Ya., Berg, G.A., Volkova, L.I. and Sokolova, V.I. "Development of hydrodesulphurization catalysts for residual petroleum feedstocks"; Chem Tech Fuels and Oils; 11:9; 1975.

19. Ashley, J.H., and Mitchell, P.C.H. "Cobalt-molybdenum-alumina hydrodesulphurization catalysts. I. Spectroscopic study of the fresh catalyst and model compounds". J Am Chem Soc A; 2821; 1968; "Cobalt-molybdenum-alumina catalyst II. Incorporation of Co (II) and Mo (VI) into Al_2O_3" ibid.; 2730; 1969.

20. Schuit, G.C.A., and Lipsch, J.M.J.G. "The CoO MoO_3 system"; J Catal; 15:163; 1969.

21. Krylov, O.V. and Margolis, L.Y. "Complexing of mixed oxide catalysts"; Kinet and Katal; 11:432; 1970.

22. Ratnasamy, P., Mehrotra, R.P., and Ramaswamy, A.V. "Interaction between the active components and support in Co-Mo-Al_2O_3 systems"; J Catal; 32:63; 1974.

23. Ochoa, O., Galiasso, R., and Andreu, P. "Study of some variables involved in the preparation of impregnated catalysts for hydrotreating heavy oils"; Studies in Surface Science Catalysis; 13:493; 1979.

24. Kotera, Y., Todo, N., Muramatsu, K., and Ogawa, K. "Hydrodesulphurization catalysts for residual oil - I. Preparation and its effects on the HDS activity of Co-Mo-Al_2O_3 catalysts"; Kogyo Kagaku Zasshi; 74:330; 1971.

25. Delmon, B., Jacobs, P.A. and Poncelet, G. eds. "Preparation of catalysts"; Elsevier, New York; 1976.

26. Anderson, R.B. "Experimental methods in catalytic research"; Academic Press, New York; 1968.

27. Ozubko, R.S. "Quantitative analysis of heavy fossil fuels using H^1 and C^{13} FTNMR analyses"; Contract Report 93945; CANMET, Energy, Mines and Resources Canada; 1978.

28. Gitzen, W.H. "Alumina as a ceramic material"; Am Ceram Soc; Special Publication No. 4, Columbus, Ohio; 1970.

29. Wells, A.F. "Structural inorganic chemistry"; Clarendon Press, Oxford; 1962.

30. Lo Jacono, M., and Schiavello, M. "The influence of preparation methods on structural and catalytic properties of transition metal ions supported on alumina"; Ref. 25:473.

31. Bancroft, G.M., Gupta, R.P., Hardin, A.H. and Ternan, M. "Quantitative electron spectroscopy for chemical analyses of bitumen processing catalysts"; Anal Chem; 51:2102; 1979.

32. Pollock, S.S., Yeu, T.F., and Erdman, J.G. "Investigation of the structure of petroleum asphaltenes by X-ray diffraction"; Anal Chem; 33:1587; 1961.

33. Riediger, B. "Demetallization, detarring and desulphurization of distillation residues"; Intern Chem Eng; 16:203; 1976.

34. Makhija, R., Draper, R.G., and Furimsky, E. "Rapid method for determining sulphur and vanadium in petroleum products by non-dispersive X-ray fluorescence"; CANMET Report 77-61; Energy, Mines and Resources Canada; 1977.

35. Oleck, S.M. and Sherry, H.S. "Fresh water manganese nodules as a catalyst for demetallizing and desulphurizing petroleum residue"; Ind Eng Chem Proc Des Dev; 16:525; 1977.

36. Kurita, S., Watanabe, T., and Takayama, N. "Hydrodesulphurization of thiophene I. Effect of coke deposition on catalyst reaction rates"; Bull Pet Inst; 13:169; 1971.

37. Mosby, J.F., Hockstra, G.B., Kleinhenz, T.A. and Sroka, J.M. "Pilot plant proves residue process"; Hydrocarbon Process; 93; May 1973.

38. Furimsky, E. "Deactivation and regeneration of refinery catalysts"; Erdol Und Kohle - Erdgas; 32:383; 1979.

39. Bell, A.T. and Somorjai, G. eds. "Preprints of the conference on catalyst deactivation and poisoning"; Lawrence Livermore Laboratory, Publication No. 238; Berkley; May 1978.

40. Constantinides, G. and Arich, G. "Research on metal complexes in vacuum resids"; Proc Sixth World Petrol Congr; 2:65; 1963.

41. Treibs, A. "Chlorophyll and hemin derivatives in organic mineral substances"; Angew Chem; 49:682; 1936.

42. Krejci-Grat, K. "Moderne anschauungen uber die entstehung des erdols"; Erdoel und Kohle; 13:836; 1960.

43. Qader, S.A., Singh, S., Wiser, W.H. and Hill, G.R. "Hydrocracking of petroleum oils"; J Inst Pet London; 56:187; 1970.

44. Katsobashvili, R. Ya. "Composition of coke deposits formed in hydrocracking at low pressures"; Chem Tech Fuels and Oils; 5:698; 1969.

45. Ternan, M., Furimsky, E. and Parsons, B.I. "Coke formation on HDS catalysts"; Fuel Proc Technol; 2:45; 1979.

46. Aitken, A.R., Merrill, W.H., Pleet, M.P., Fulford, G.N. and Parsons, B.I. "Comparison of the high pressure hydrogenating characteristics of cobalt molybdate catalysts with different pore volume distributions"; Internal Report FMP 62/40-HPC, Fuels and Mining Practise Division; Dept of Mines and Technical Surveys; Ottawa; 1962.

47. Montgomery, D.S., Parsons, B.I. and Machin, W.D. "Process for the preparation of metal oxides having an enlarged pore volume"; Can Patent; 748,798, 1963.

48. Shaw, G.T. and Parsons, B.I. "Low density catalysts and catalyst supports, Part I, The preparation of highly porous alumina"; Research Report R199; Mines Branch; Energy, Mines and Resources Canada; 1968.

49. Shah, Y.T. and Paraskos, J.A. "Intraparticle diffusion effects in residue HDS"; Ind Eng Chem Proc Des Dev; 14:368; 1975.

APPENDIX A

CATALYST MEASUREMENTS

AND

PROPERTIES OF THE LIQUID PRODUCT

Table A-1 - Catalyst measurements

Catalyst MB No.	Calcin'g temp. (°C)	Calcin'g time (h)	Surface area (m^2/g)	Median pore diam (nm)	Catalyst in reactor	Fresh catalyst			Used catalyst		
						MoO_3 (*m* %)	CoO (*m* %)	Al_2O_3 (*m* %)	Carbon (*m* %)	Hydrogen (*m* %)	Nitrogen (*m* %)
Alumina catalyst - without other components											
357	600	2	166	7.8	71.68	0.135	0.05	87.57	12.99	1.30	0.32
358	900	2	96	12.0	80.12	0.406	0.06	91.13	8.44	0.92	0.15
361	1050	0.5	58	16.0	86.01	0.947	0.09	94.53	5.98	0.65	0.17
419	1100	2	23	29.0	105.05	0.030	-	96.17	3.87	0.31	0.09
359	1050	2	18	55.0	89.32	1.292	0.08	96.46	1.47	0.13	0.03
2.2 *m* % MoO_3:1.1 *m* % CoO on alumina											
415	600	2	188	7.2	64.01	2.104	1.03	83.89	10.69	1.20	0.31
416	600	2	188	7.2	64.01	1.97	1.06	88.27	11.88	1.31	0.32
367	600		176	7.5	74.78	2.09	0.98	86.55	10.50	1.28	0.27
379	700		157	8.5	73.45	2.30	0.99	87.44	9.95	1.13	0.27
381	800		118	10.0	79.68	2.04	0.99	89.92	7.79	0.87	0.20
382	850		99	12.5	76.03	2.06	0.99	91.49	7.82	0.84	0.19
418	950	2	80	15.3	64.01	2.06	1.09	91.69	7.72	0.83	0.19
417	950	2	78	15.5	64.01	2.16	1.08	91.37	7.62	0.69	0.20
384	875		79	16.0	78.97	2.07	1.00	91.30	7.18	0.75	0.18
420	1030	2	40	28.0	84.20	2.12	1.09	92.18	5.50	0.46	0.15
380	950		45	28.5	85.35	2.25	1.11	93.96	5.14	0.48	0.14
368	900		38	37.5	92.54	4.31	1.03	90.7	5.04	0.48	0.15
383	1000		32	50.0	86.20	2.16	1.03	93.60	3.59	0.31	0.09
371	1050		8	1180.0	88.66	1.95	1.07	95.42	0.44	0.03	-
369	1050		<2	3000.0	85.96	1.28	0.41	97.19	0.31	0.02	-
8.8 *m* % MoO_3:4.4 *m* % CoO on alumina											
362	600	2	185	6.5	81.65	7.78	4.02	78.71	-	-	-
398	700	2	162	7.8	80.96	7.93	4.07	78.99	10.38	0.59	0.34
									9.11	1.15	0.33
402	735	2	94	14.0	83.80	8.10	4.20	80.13	12.87	0.71	0.31
									8.97	0.93	0.32
399	775	2	70	21.2	87.40	8.31	4.14	82.19	10.18	1.09	0.33
									6.89	0.70	0.25
365	800	2	57	28.8	89.58	8.16	4.37	84.53	6.09	0.71	0.28
401	825	2	28	38.0	97.44	7.87	4.41	85.08	8.67	0.80	0.26
									5.36	0.49	0.19
403	950	1	18	88.0	96.34	8.10	4.42	84.34	8.92	0.79	0.27
									3.29	0.26	0.11
400	850	2	4	490.0	91.93	7.65	4.60	86.69	6.19	0.56	0.13
									0.96	0.06	0.02
400(2)	850	2	2	530.0	87.65	7.57	4.54	87.63	6.89	0.61	0.20
									1.74	0.12	0.09
363	900	2	<1	600.0	95.28	7.54	4.55	87.31	0.72	0.07	0.2
364	1050	2	<1	5500.0	112.26	4.70	4.59	90.67	4.25	0.38	0.09
									0.40	0.03	0.01
365	1050	0.5	<1	5500.0	109.27	6.94	4.55	86.21	3.87	0.34	0.08
									0.52	0.03	0.01
15 *m* % MoO_3:3 *m* % CoO on alumina											
426	600	2	199	5.4	83.22	13.48	2.80	73.19	10.24	1.17	0.43
372	600	2	190	6.6	88.09	13.61	2.61	75.52	7.23	1.02	0.35
376	660	2	90	14.0	102.05	13.58	2.73	76.57	9.04	0.82	0.31
427	700	2	61	19.0	84.71	14.33	2.81	77.07	6.60	0.66	0.26
422	775	2	54	20.5	87.09	13.99	2.86	75.57	6.53	0.62	0.24
423	790	2	44	23.0	95.14	14.46	2.98	78.05	6.79	0.57	0.22
374	700	2	47	25.0	95.30	14.06	2.87	78.09	6.50	0.52	0.23
405	725	2	40	29.0	104.38	14.03	2.80	77.52	4.89	0.44	0.16
375	750	2	24	38.0	116.38	13.72	2.87	79.26	3.36	0.29	0.13
404	800		3	400.0							
373	900	2	<1	3700.0	132.78	6.03	2.76	89.50	0.29	0.03	-
429	850	2	<1	10,000.0							
431	950	2	<1	10,000.0							
430	900	2	<1	11,400.0							

(2) indicates second batch of catalyst

Table A-2 - Properties of the liquid product

Cat MB No.	Run number LPH	Yield (*m* %)	Relative density	S (*m* %)	Mi (*m* %)	C (*m* %)	H (*m* %)	Benzene insol. (*m* %)	Pentane insol. (*m* %)	+525°C Pitch (*m* %)	Va (*m* %)	Ni (*m* %)	Fe (*m* %)
Steel extrudates													
	1168	93.98	0.960	3.51	0.38	84.33	10.50	1.68	10.80		230	72	282
Alumina catalyst - Without other components													
357	1070	95.47	0.960	3.53	0.34	85.26	10.66	0.77	9.39	32.65	118	56	67
358	1074	94.98	0.945	2.37	0.30	85.04	11.06	0.40	6.35	29.45	72	37	325
361	1098	94.80	0.931	2.02	0.32	85.49	11.34	0.34	5.79	27.65	68	24	287
419	1160	90.14	0.933	2.80	0.34	85.20	11.01	0.84	6.44	20.48	92	41	321
359	1080	97.51	0.942	2.02	0.33	85.24	11.04	0.41	6.07	30.52	54	25	324
2.2 *m* % MoO_3:1.1 *m* % CoO on alumina													
415	1138	91.70	0.913	1.06	0.31	86.82	11.71	0.17	3.79	19.32	36	20	352
416	1142	92.67	0.913	0.82	0.31	87.06	11.77	0.22	2.86	21.05	19	13	299
367	1064	91.28	0.926	1.34	0.27	85.88	11.41	0.70	5.44	25.86 22.90	50	24	31
379	1086	93.42	0.912	0.92	0.26	86.50	11.62	0.68	4.56	16.99	41	20	407
381	1092	91.61	0.917	0.97	0.26	86.63	11.61	0.49	4.11	17.84	40	20	372
382	1090	93.66	0.920	0.92	0.27	86.46	11.52	0.53	3.99	17.64	40	19	389
418	1144	94.89	0.921	0.96	0.33	87.03	11.73	0.27	3.62	25.45	25	16	344
417	1140	91.22	0.907	0.96	0.31	86.96	11.74	0.46	3.48	14.40	28	12	317
384	1096	93.73	0.929	1.25	0.30	86.14	11.49	0.49	4.68	24.16 25.16	46	23	383
420	1162	91.97	0.905	1.25	0.36	86.10	11.70	0.16	3.28	15.62	21	12	332
380	1088	93.35	0.920	1.18	0.30	86.23	11.46	0.40	4.25	22.69	40	20	304
368	1072	93.88	0.922	0.97	0.28	87.40	11.62	0.44	3.88	21.82	30	18	312
383	1094	93.43	0.927	1.40	0.31	86.16	11.45	0.34	4.43	21.34	40	21	296
371	1084	95.76	0.960	3.17	0.37	86.50	11.62	0.37	8.12	26.39	115	43	349
369	1082	90.22	0.968	3.68	0.39	84.30	10.59	0.49	9.42	22.27	158	62	396
8.8 *m* % MoO_3:4.4 *m* % CoO on alumina													
362	1066	94.24	0.914	0.92	0.21	86.56	11.80	0.75	4.67	24.81	39	19	8
398	1115	103.16	0.911	0.69	0.23	82.99	11.35	0.73	3.48	10.65	41	18	427
402	1130	85.92	0.877	<0.20	0.09	87.85	12.09	0.49	1.38	0.06	15	9	387
399	1124	91.98	0.905	0.43	0.13	87.07	11.64	-	1.79	10.76	24	12	358
365	1100	94.69	0.911	0.85	0.19	86.72	11.72	0.46	3.40	13.36	32	15	304
401	1128	91.91	0.912	0.83	0.27	87.22	11.66	0.54	3.69	10.47	36	17	312
403	1132	95.20	0.910	0.84	0.31	87.09	11.46	0.82	3.77	7.05	46	24	528
400	1126	93.57	0.941	2.59	0.33	85.99	11.00	0.74	7.50	15.32	101	44	345
400(2)	1134	85.66	0.924	2.25	0.37	86.24	11.01	1.12	6.11	8.31	82	38	295
363	1076	93.68	0.953	3.28	0.34	85.61	11.35	0.39	8.47	23.32	121	46	34 24
364	1118	95.02	0.955	3.38	0.37	85.24	10.69	1.08	8.58	21.35	147	45	160
365	1122	93.62	0.952	3.13	0.37	85.20	10.66	0.97	8.56	17.84	147	48	279
15 *m* % MoO_3:3 *m* % CoO on alumina													
426	1170	97.52	0.908	0.86	0.16	86.17	11.81				50	20	436
372	1068	94.25	0.910	0.73	0.18	85.05	11.53	0.47	4.67	23.08	52	22	362
376	1156	88.88	0.891	0.96	0.13	87.00	12.12	0.32	2.11	11.85	15	8	288
427	1172	96.55	0.911	1.06	0.22	86.63	11.98				34	16	442
422	1164	92.22	0.903	0.98	0.26	87.02	11.91	0.49	3.94	11.73	18	12	243
423	1166	89.11	0.903	0.81	0.14	87.04	11.89	0.41	2.57	17.69	16	10	147
374	1154	92.09	0.902	0.84	0.26	87.14	11.97	0.39	2.51	16.47	19	11	380
405	1158	91.65	0.901	1.13	0.17	86.52	11.91	0.54	3.14	15.67	19	11	303
375	1048	94.07	0.916	1.22	0.30	86.54	11.69	0.44	4.19	21.65	38	18	384
373	1078	105.91	0.965	3.68	0.35	83.72	10.36	0.47	9.86	34.42	188	66	406

(2) indicates second batch of catalyst

OPINION POLL

The opinion of concerned readers may influence the direction of future CANMET research.

We invite your assessment of this report - No._____

Is it useful?	Yes_____	No_____
Is it pertinent to an industry problem?	Yes_____	No_____
Is the subject of high priority?	Yes_____	No_____

Comments_____

_____

_____

Please mail to: CANMET Editor, EMR, 555 Booth Street, Ottawa, Ontario, K1A 0G1

A complimentary copy of the CANMET REVIEW describing CANMET research activity will be sent on request.

CANMET REPORTS

Recent CANMET reports presently available or soon to be released through Printing and Publishing, Supply and Services Canada (addresses on inside front cover), or from CANMET Publications Office, 555 Booth Street, Ottawa, Ontario, K1A 0G1:

Les récents rapports de CANMET, qui sont présentement disponibles ou qui le seront bientôt peuvent être obtenus de la direction de l'Imprimerie et de l'Edition, Approvisionnements et Services Canada (adresses au verso de la page couverture), ou du Bureau de Vente et distribution de CANMET, 555 rue Booth, Ottawa, Ontario, K1A 0G1:

80-12F Ressources Canadiennes en rebuts minéraux rapport No. 4 - Les rebuts minéraux dans les provinces Atlantiques; R.K. Collings;
Cat. No. M38-13/80-12F, ISBN 0-660-90775-5; Price: $1.95 Canada, $2.35 other countries.

80-13F Ressources en rebuts minéraux au Canada rapport No. 6 - Rebuts minéraux employés comme chargés; R.K. Collings;
Cat No. M38-13/80-13F, ISBN 0-660-90790-9; Price: $2.25 Canada, $2.70 other countries.

80-17F Revue de CANMET 1979-80; Staff of Technology Information Division;
Cat. No. M38-13/80-17F, ISBN 0-660-90789-5; Price: $5.00 Canada, $6.00 other countries.

80-20E An iris diaphragm-based interface for use in eriometry; B. Kirk;
Cat. No. M38-13/80-20E, ISBN 0-660-10914-X; Price: $2.50 Canada, $3.00 other countries.

80-26E Release of Lead from typical Canadian Pottery glazes; D.H.H. Quon and K.E. Bell;
Cat. No. M38-13/80-26E, ISBN 0-660-10902-6; Price: $1.75 Canada, $2.10 other countries.

80-27E Generation and control of mine airborne dust; G. Knight;
Cat. No. M38-13/80-27E, ISBN 0-660-10958-1; Price: $2.10 Canada, $2.50 other countries.

81-1E Niobium ore OKA-1 - A certified reference material; H. Steger and W.S. Bowman;
Cat. No. M38-13/81-1E, ISBN 0-660-10915-8; Price: $1.75 Canada, $2.10 other countries.

81-2E Acid extraction of alumina from Canadian non-bauxite sources at CANMET; Colin Hamer;
Cat. No. M38-13/81-2E, ISBN 0-660-10957-3; Price: $2.00 Canada, $2.40 other countries.

81-3E Feasibility study on recovery of thermal coal from waste dumps in Nova Scotia; M.W. Mikhail, L.C. Bird and N.T.L. Landgren;
Cat. No. M38-13/81-3E, ISBN 0-660-11007-5; Price: $3.75 Canada, $4.50 other countries.

81-4E Effect of Pore Size in MoO_3-CaO-Al_2O_3 Hydrocracking Catalysts;
A.H. Hardin, M. Ternan and R.H. Packwood;
Cat. No. M38-13/81-4E, ISBN 0-660-11065-2; Price: $3.75 Canada, $4.50 other countries.

81-5E High performance liquid chromatographic method for type analysis of hydrocarbons in synthetic fuel naphtha; J.E. Beshai and A.E. George;
Cat. No. M38-13/81-5E, ISBN 0-660-10985-9; Price: $1.50 Canada, $1.80 other countries.